The Astrophysical Journal, 589:931–952, 2003 June 1

GAS IN THE TERRESTRIAL PLANET REGION OF DISKS: CO FUNDAMENTAL EMISSION FROM T TAURI STARS

Joan Najita
NOAO, 950 North Cherry Avenue, Tucson, AZ 85719; najita@noao.edu

John S. Carr
Naval Research Laboratory, Code 7213, Washington, DC 20375; carr@mriga.nrl.navy.mil

and

Robert D. Mathieu
Department of Astronomy, University of Wisconsin, Madison, WI 53706; mathieu@astro.wisc.edu
Received 2002 November 14; accepted 2003 February 17

ABSTRACT

We report the results of a high-resolution spectroscopic survey for CO fundamental emission from T Tauri stars. CO fundamental emission is frequently detected, with the likely origin of the emission in the circumstellar disk. An initial assessment of the line profiles indicates that the emission region includes the equivalent of the terrestrial planet region of our solar system, a result that suggests the utility of CO fundamental emission as a probe of disks at planet formation distances. Since fundamental emission is detected frequently from both close binary and apparently single stars, it appears that both low column density regions, such as disk gaps, and temperature inversion regions in disk atmospheres can produce significant emission. The estimated excitation temperature of the emitting gas is unexpectedly warm for the disk radii that they appear to probe. Thus, the surface gaseous component of inner disks may be significantly warmer than the surface dust component. We also detect CO emission from a transitional T Tauri star. Because fundamental emission from CO and its isotopes is sensitive to a wide range of gas masses, including masses $\ll M_{\oplus}$, CO fundamental emission may prove useful in measuring the residual gas content of dissipating disks. This may be an effective way to explore the gas dissipation timescale in inner disks and to thereby place constraints on the timescale for giant planet formation.

Subject headings: circumstellar matter — planetary systems: formation — planetary systems: protoplanetary disks — stars: variables: other

1. INTRODUCTION

As the likely birthplaces of planets, the inner regions of young circumstellar disks have long been regarded as potential analogs of the protosolar nebular regions in which Jupiter and the terrestrial planets formed. Thus, there is considerable motivation to develop spectral line diagnostics of this region in order to study the physical and dynamical conditions under which planetary systems form. The motivation to study inner disks is all the more intense today given the discovery of planets outside the solar system. The properties of the extrasolar planetary systems have revealed a tremendous diversity that was unanticipated by traditional planet formation theory. In particular, there is an abundance of giant planets spread over a range of orbital radii less than 5 AU, which highlights the possibility of significant orbital migration through the inner disk region in the early evolution of planetary systems. These developments further highlight the need for observational probes of inner disks that may help to guide the development of a predictive theory of the formation and evolution of planetary systems.

The exploration of the inner disk region ($r \lesssim 5$ AU) is challenging at present because of the small angular scales subtended by the inner disk at the distance of the nearest star-forming regions ($\lesssim 0\farcs03$ at 150 pc). As a result, studies of inner disks are currently restricted to the realm of high-resolution spectroscopy, where, in principle, high velocity resolution can be employed in lieu of high spatial resolution to measure the properties of disks over a range of radii. For this purpose, infrared spectroscopy of molecules is well suited as a probe of the warm ($T \gtrsim 150$ K), dense ($n = 10^9$–10^{15} cm^{-3}) conditions in inner disks (see Najita et al. 2000 for a review). At these temperatures, molecules such as CO and water are expected to be abundant and fully in the gas phase. Consequently, processes such as adsorption on grain surfaces, which complicates the measurement of gas column densities in the cooler outer disk (e.g., Dutrey et al. 1996), are not expected to be a concern. The warm temperatures and high densities characteristic of inner disks are also expected to excite a rich spectrum of molecular vibrational-rotational transitions that can be used to deduce the physical conditions of the gas from which they arise. The specific conditions required to excite these transitions limit the possible physical origin of the emission to a few components of the young stellar environment (e.g., inner disk, inner wind, and funnel flow). These possibilities can be distinguished with measured line profiles.

At the large column densities generally expected for the inner disk ($\sim$1500 g cm^{-2} at 1 AU for the minimum-mass solar nebula), the disk will be optically thick in the continuum. As a result, emission and absorption features are expected from regions with significant vertical temperature structure, i.e., from disk atmospheres. A good illustration is provided by Calvet et al. (1991), who have shown that accretion in the disk midplane, in the presence of stellar irradiation of the disk surface, can produce both emission and absorption features in the 2.3 μm CO overtone bands,

depending on the relative strength of the accretion compared to the irradiating flux. Apart from an origin in disk atmospheres, strong line emission may also be produced in regions of low continuum optical depth, e.g., low column density regions of the disk cleared dynamically by the presence of stellar or planetary companions, where residual gas may produce bright line emission against the weak continuum emission from the region.

Examples of each of these cases have been reported in the literature. High-resolution ($R \sim 20,000$) spectroscopy of CO overtone emission from young stars reveals that the emission often has the characteristic spectral shape of bandhead emission from a rotating disk (Carr et al. 1993; Najita et al. 1996; see also Chandler, Carlstrom, & Scoville 1995). A disk signature is particularly apparent in the case of the hotter, more massive young stars ($M_* > 1\ M_\odot$) in which CO absorption from the stellar photosphere, being absent, does not complicate the line profile. Because the overtone-emitting sources have large near-infrared excesses indicative of optically thick inner disks, the emission is believed to arise in a disk atmosphere. Large gas column densities ($\sim$0.1–1000 g cm^{-2}) are required to produce the strength and shape of the overtone emission, with the bulk of the emission originating within $\sim$0.2 AU for the lower mass ($\sim 1\ M_\odot$) objects.

Emission lines of hot water vapor have also been detected in high-resolution spectra of young stars in the 2 μm region (see Najita et al. 2000). The water emission is also believed to arise from a disk temperature inversion region for the same reason given for the CO overtone emission. Comparing the widths of the CO overtone and hot water lines in sources in which both lines are detected, the CO overtone lines are found to be broader than the water lines. Since the dissociation temperature for water is lower than that for CO, this trend is consistent with a common origin for both lines in a Keplerian disk with an outwardly decreasing temperature profile. The water emission spectrum can be quite dense in some spectral regions, potentially creating a pseudocontinuum that can complicate the detection and identification of weak emission features of water as well as other molecules.

These results illustrate the potential of high-resolution spectroscopy to probe the dynamics and physical conditions of inner disks. One limitation of these results is that both the hot water lines in the 2 μm region and the CO overtone emission probe very warm gas, $\gtrsim$2000 K. As a result, these diagnostics only probe the region of the disk very close to the star, $\lesssim$0.2 AU. Thus, there is considerable interest in being able to make similar measurements at lower gas temperatures and larger disk radii.

Along these lines, we have also previously reported high-resolution spectroscopy of CO fundamental emission from the T Tauri spectroscopic binary system DQ Tau (Carr, Mathieu, & Najita 2001). Close binary systems like DQ Tau are attractive systems in which to search for strong molecular emission because the tidal interaction of the binary with the disk is expected to reduce the column density of the disk in the vicinity of the binary orbit, creating a "gap" between the outer circumbinary disk and inner circumstellar disks. If the gap retains some residual gas, the gas will appear bright in emission against the weak continuum emission from the gap, an expectation which was confirmed in our study of the DQ Tau system. There we showed that both the excitation temperature and the width of the CO fundamental emission from the system located the emitting gas in the vicinity of the gap. Because the A-values of the fundamental transitions are large, we were able to measure strong emission from a tiny mass of gas, only $10^{-5}\ M_\oplus$.

In this paper, we broaden our study of CO fundamental emission to a larger number of systems, both binaries and apparently single stars. We report observations of CO fundamental emission from a small sample of T Tauri stars, primarily spectroscopic binary systems. These data, obtained with CSHELL at the NASA Infrared Telescope Facility, were acquired primarily to test the hypothesis that low column density regions, such as the large disk gaps that are expected to be cleared by binaries, will produce detectable CO fundamental emission. We also report the results of a more extensive NIRSPEC/Keck survey for fundamental emission from T Tauri stars, both those with and those without known companions. These data allow us to explore in greater detail the utility of CO fundamental emission as a probe of disks at planet formation distances.

2. OBSERVATIONS

2.1. *CSHELL*

High-resolution ($R = 20,000$; 1″ slit) spectra of eight T Tauri stars were obtained over four observing seasons (1995–1998) using CSHELL, the facility cryogenic infrared spectrograph at the NASA Infrared Telescope Facility (Tokunaga et al. 1990; Greene et al. 1993). We observed three known spectroscopic binaries (DQ Tau, GW Ori, and UZ Tau E), two more widely separated binaries (DF Tau and GG Tau), and, for comparison, three objects that are not known to have close companions (CW Tau, DG Tau, and RY Tau; see Table 1). The

TABLE 1
Sources Observed

Source	A_V	Binary Separation[a]	CSHELL[b]	NIRSPEC[b]
BP Tau	0.49	...	...	e
CW Tau	2.29	...	ea	ea
CY Tau	0.10	...	...	e
DF Tau	0.21	0.″088	e	e
DG Tau[c]	...	...	ea	...
DQ Tau	0.97	15.8 days	e	ea
GG Tau	0.76	0.″288	x	e
GK Tau	0.87	2.″4	...	ea
GM Aur	0.14	...	...	x
GW Ori	0.82	242 days	e	e
IQ Tau	1.25	...	...	ea
LkCa 15	0.62	...	...	e
RW Aur	...	0.″12/1.″5	...	e
RY Tau	1.84	...	a	...
UZ Tau E	1.49	19.1 days	e	e
V410 Tau	0.03	0.″123	...	x
V836 Tau	0.59	...	...	e
ZZ Tau	1.32	0.″029	...	x

[a] Either the orbital period (days) or angular separation (arcseconds).

[b] An "e" indicates detected emission, an "x" indicates no detected emission, an "a" indicates detected absorption, and an ellipsis indicates that the source was not observed.

[c] Spectral synthesis modeling shows that the observed spectrum is consistent with strong, broad emission from a rotating disk that results in significant line blending. See § 5.1.

TABLE 2
CSHELL Observations

Source	CO Line	UT Date
CW Tau	1–0 $R(3)$	1997 Jan 25
DF Tau	1–0 $R(3)$	1995 Jan 25
DG Tau	1–0 $R(3)$	1997 Jan 27
DQ Tau	1–0 $R(3)$	1995 Jan 25
	1–0 $R(3)$	1996 Jan 16
	1–0 $R(3)$	1998 Jan 8
	1–0 $P(18)$	1998 Jan 10
GG Tau	1–0 $R(3)$	1996 Jan 17
GW Ori	1–0 $R(3)$	1995 Jan 27
	1–0 $R(3)$	1996 Jan 16
	1–0 $R(6)$	1996 Jan 16
	1–0 $P(18)$	1996 Jan 17
RY Tau	1–0 $R(3)$	1997 Jan 25
UZ Tau E	1–0 $R(3)$	1996 Jan 17

observations were carried out in January in order to maximize the velocity shift of the T Tauri CO emission lines relative to telluric CO absorption (20–40 km s^{-1}). A reasonable velocity shift was particularly important for the low-J CO $v = 1$–0 (hereafter 1–0) line observations. With CSHELL, circular variable filters are used as order-sorting filters to isolate a single echelle order on the 256×256 SBRC InSb array. As a result, typically only a single CO 1–0 transition can be observed in a given spectral setup. The sources, dates of observation, and spectral settings are listed in Table 2. The results for DQ Tau have been reported in a previous publication (Carr et al. 2001) but are included here for completeness.

The telescope was nodded between integrations in order to alternately place the object at two positions on the slit separated by $\sim 15''$. The spectra from each beam were extracted and corrected for telluric absorption by dividing by the spectrum of a hot star (either HR 1412 or HR 1790). Telluric lines in the spectra were used for the wavelength calibration. With the exception of the GW Ori and DQ Tau $R(3)$ spectra taken in 1995, the spectra were flux-calibrated with additional spectra of the target star and the telluric standard taken through a $4''$ slit. The resulting calibrated spectra, for the sources in which either emission or absorption was detected, are shown in Figure 1.

2.2. *NIRSPEC*

We also obtained high-resolution ($R = 23,000$) spectra of a larger sample of T Tauri stars, both single stars and binaries, with NIRSPEC (see Table 1), the facility cryogenic infrared echelle spectrometer on the Keck II telescope (McLean et al. 1998, 2000). The stars in the sample span a range in activity, with stellar accretion rates from the literature ranging from as high as 4×10^{-7}, or more, to less than $10^{-9}\ M_{\odot}\ \mathrm{yr}^{-1}$ (see § 5.2). The observations were carried out in echelle mode with the $0''.43$ slit. Since NIRSPEC is cross-dispersed and is equipped with a large-format detector (1024×1024 ALADDIN InSb), multiple orders are accessible simultaneously. As a result, we are able to observe in a single spectral setting both the low-J CO 1–0 R-branch transitions at 4.6 μm and the high-J CO 1–0 P-branch transitions at 4.9 μm.

Prior to our observing run, it was discovered that degradation of the NIRSPEC Dewar window led to the production of spurious thermal sources that did not subtract well in observations taken with the image rotator. As a result, we carried out the observations in "stationary guiding mode" (i.e., with the image rotator turned off). The telescope was nodded by hand between integrations in order to place the object at two positions along the $\sim 24''$ slit. The spurious thermal sources subtracted well in the resulting pair-differenced images.

An additional difficulty was the "fixed pattern" noise in two quadrants of the detector. Because we used a large number of co-adds, as is required for M-band spectroscopy, the fixed pattern noise was significant, effectively reducing the signal-to-noise ratio (S/N) in the spectra falling on the short-wavelength half of the array. To contend with the fixed pattern noise, we altered our spectral setting on the latter two nights of observations. The spectra obtained on 2001 January 19 and 20 cover the regions 4.587–4.662 and 4.890–4.970 μm. The spectra obtained on 2001 January 17 cover the regions 4.613–4.670 and 4.919–4.997 μm. The sources and dates of observation are listed in Table 3.

The spectra from each beam were extracted and corrected for telluric absorption by dividing by the spectrum of a hot star (HR 1412, HR 4343, or HR 3192). The hot-star spectra are generally featureless, except for the 7–5 Pfβ line, which appears in absorption and which we did not attempt to correct for. As a result, division by the hot-star spectrum artificially enhanced the hydrogen line emission in the resulting spectra. Telluric lines in the spectra were used for the wavelength calibration.

In order to attempt a rough flux calibration of the spectra, we acquired additional spectra of the target star and telluric standard through the largest width slit available with NIRSPEC. Although the seeing was typically $0''.5$ throughout the observations, the $0''.72$ slit was probably only marginally adequate for the flux calibration. We can obtain an estimate of the error in the flux calibration by comparing our resulting continuum fluxes with values from either the literature or our measurements with CSHELL. These comparisons are not highly reliable because T Tauri stars are notoriously variable.

TABLE 3
NIRSPEC Observations

Source	UT Date
BP Tau	2001 Jan 20
CW Tau	2001 Jan 19
CY Tau	2001 Jan 20
DF Tau	2001 Jan 19
DQ Tau	2001 Jan 17
GG Tau	2001 Jan 19
GK Tau	2001 Jan 20
GM Aur	2001 Jan 19
GW Ori	2001 Jan 19
IQ Tau	2001 Jan 20
LkCa 15	2001 Jan 19
RW Aur	2001 Jan 17
UZ Tau E	2001 Jan 17
V410 Tau	2001 Jan 20
V836 Tau	2001 Jan 20
ZZ Tau	2001 Jan 20

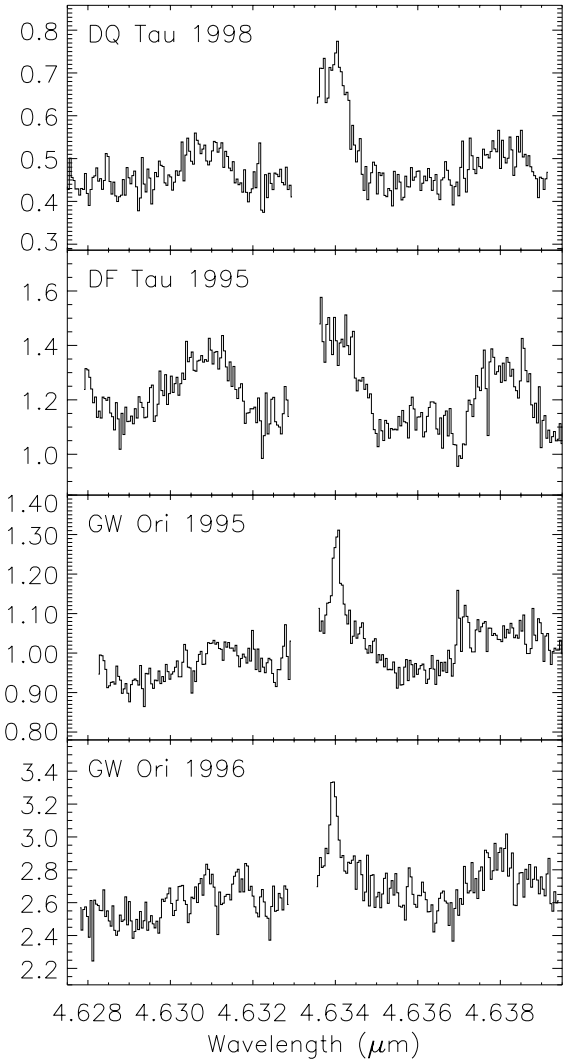

FIG. 1*a*

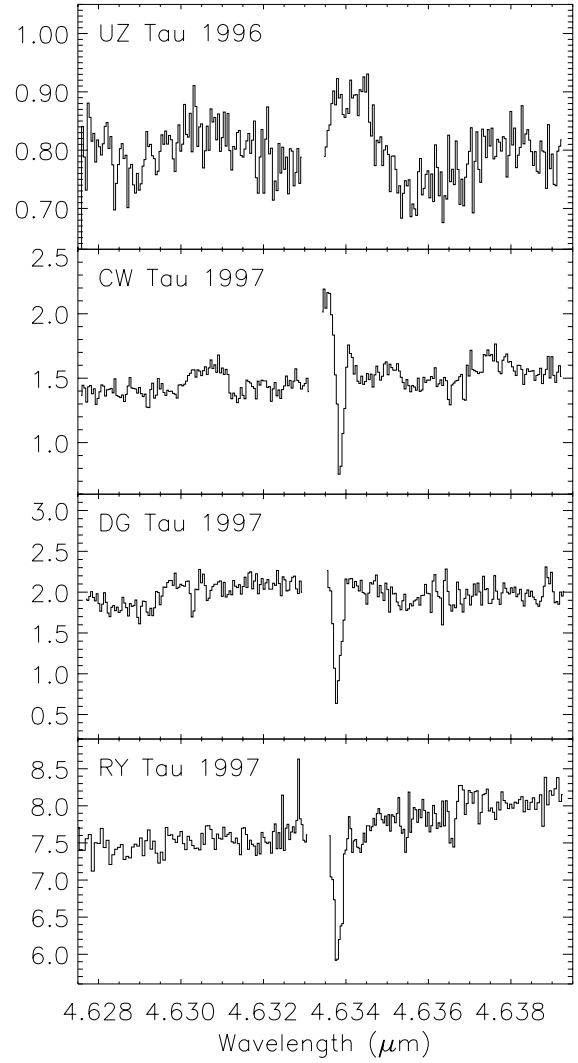

FIG. 1*b*

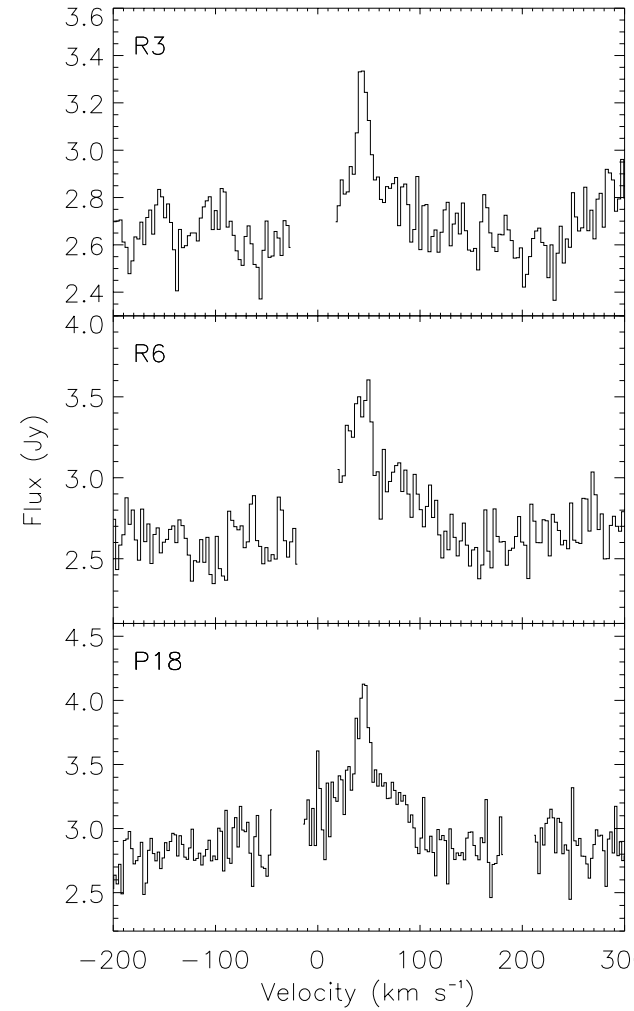

FIG. 1*c*

FIG. 1.—(*a*) CO fundamental spectra of T Tauri stars observed with CSHELL. The observations are centered on the $v = 1$–0 $R(3)$ line. Regions of strong telluric absorption have been excised from the plots. The flux scale is in Jy, except for the GW Ori 1995 spectrum, which is shown on a relative flux scale. (b) Same as (*a*), for additional stars. (*c*) Line profiles of the CO $v = 1$–0 $R(3)$, $R(6)$, and $P(18)$ emission from GW Ori, as observed in 1996 with CSHELL. Regions of strong telluric absorption have been excised from the plots.

Comparing our continuum fluxes (for BP Tau, CW Tau, DF Tau, GG Tau, GK Tau, and UZ Tau) with *M*-band fluxes from the literature (e.g., Kenyon & Hartmann 1995), the values agree to within 20%. The one exception is GG Tau, where our measured *M*-band continuum flux is only 60% of that measured by Kenyon & Hartmann (1995). Since GG Tau (Aab) has a binary separation of 0″.29 and a flux ratio of 0.45 at *L* (White et al. 1999), part of the discrepancy could be due to GG Tau Ab falling outside the slit. Comparing our *M*-band continuum fluxes for DQ Tau and GW Ori with those measured previously with CSHELL, we also find agreement to within 15%. The resulting calibrated spectra are shown in Figure 2. As is apparent from the figure, detector pattern noise in the short-wavelength half of the spectra and residuals in the telluric correction are significant sources of noise.

3. RESULTS

We find that CO fundamental line emission is frequently detected from both known binary and apparently single stars (see Table 1). At the sensitivity of NIRSPEC, fundamental emission was detected in six of the eight binaries (i.e., sources defined as having a companion within 1″; DQ Tau, UZ Tau E, GW Ori, DF Tau, GG Tau, and RW Aur). We did not detect emission from ZZ Tau and V410 Tau. Fundamental emission was also detected in seven of eight apparently single stars (i.e., sources with no known companion within 1″; BP Tau, CW Tau, CY Tau, GK Tau, IQ Tau, LkCa 15, and V836 Tau). We did not detect emission from GM Aur. We also studied two additional apparently single stars with CSHELL from which fundamental emission was not clearly detected (RY Tau and DG Tau). Since these stars were not studied with NIRSPEC, we cannot rule out the possibility of emission from these sources. In § 5.1 we show that the CSHELL spectrum of DG Tau is consistent with broad emission from warm gas that results in significant line blending. If we count this probable detection of emission from DG Tau, then CO emission was detected from 14 of the 18 sources observed.

For every source from which reasonably strong CO 1–0 emission was detected (i.e., all emission sources except IQ Tau, LkCa 15, and V836 Tau), CO $v = 2$–1 (hereafter 2–1) emission was also detected. In these sources, the 2–1 lines are considerably weaker than the 1–0 lines (typically $\sim\frac{1}{3}$ the flux). Similarly, weak 2–1 emission in IQ Tau, LkCa 15, and V836 Tau would not have been detectable

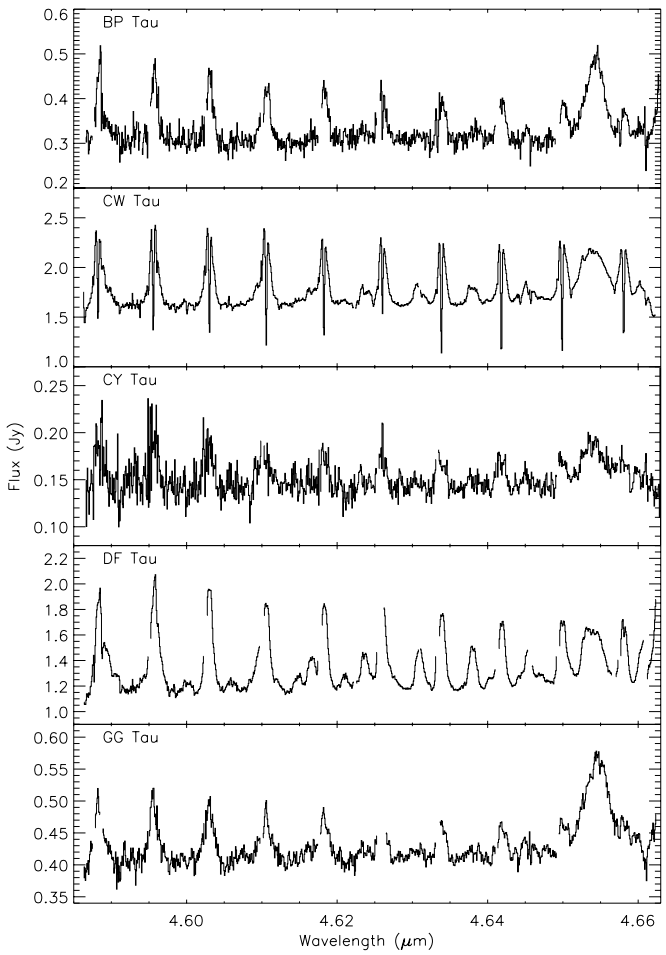

FIG. 2*a*

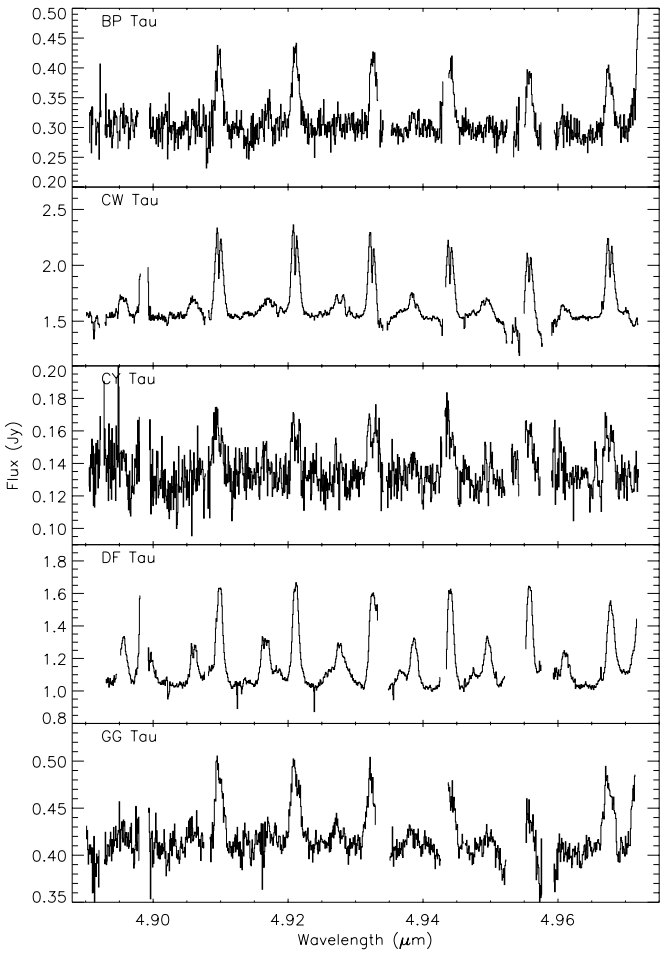

FIG. 2*b*

FIG. 2.—CO fundamental spectra of T Tauri stars observed with NIRSPEC. (*a, c, e*) The 4.6 μm region. (*b, d, f*) The 4.9 μm region. Regions of strong telluric absorption have been excised from the plots. Note that hydrogen 7–5 Pfβ absorption was present in the telluric standard used in calibrating these data. Since we did not attempt to correct for the absorption, the hydrogen line emission at ≈4.654 μm is artificially enhanced. (*g*) CO fundamental spectrum of DF Tau in the 4.6 and 4.9 μm regions. Transitions of CO 1–0, 2–1, and 3–2 and ^{13}CO 1–0 are detected in emission.

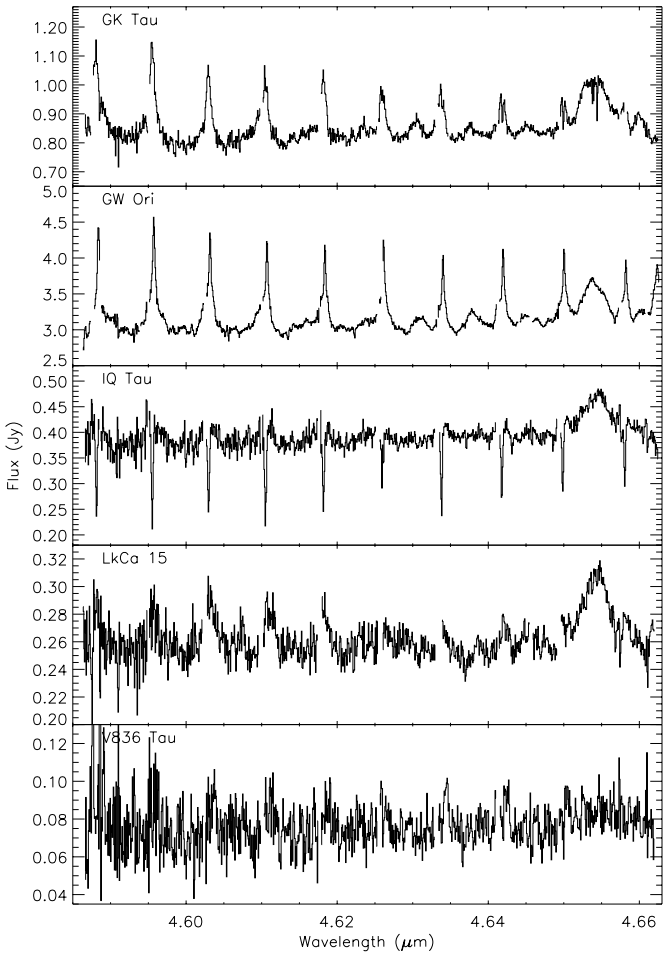

FIG. 2*c*

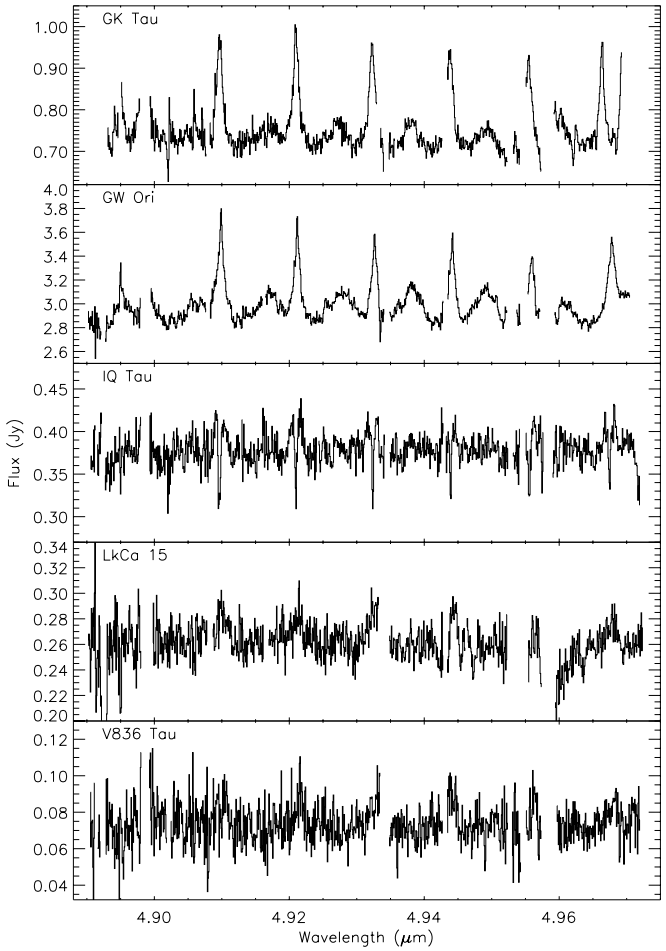

FIG. 2*d*

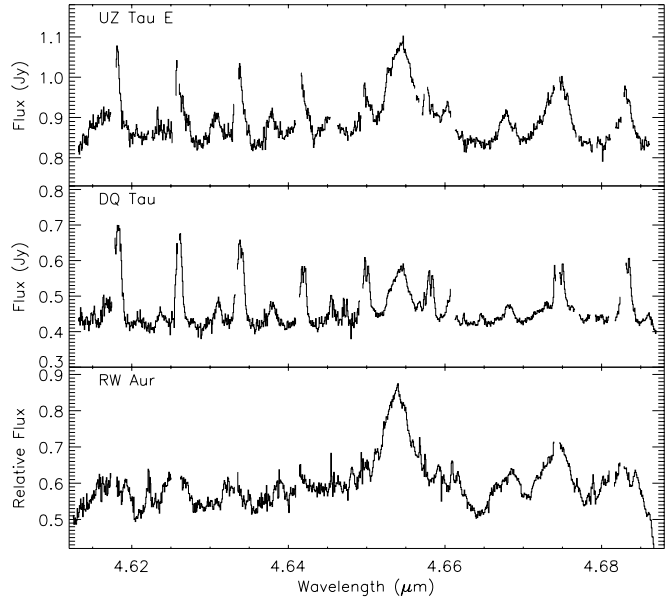

FIG. 2*e*

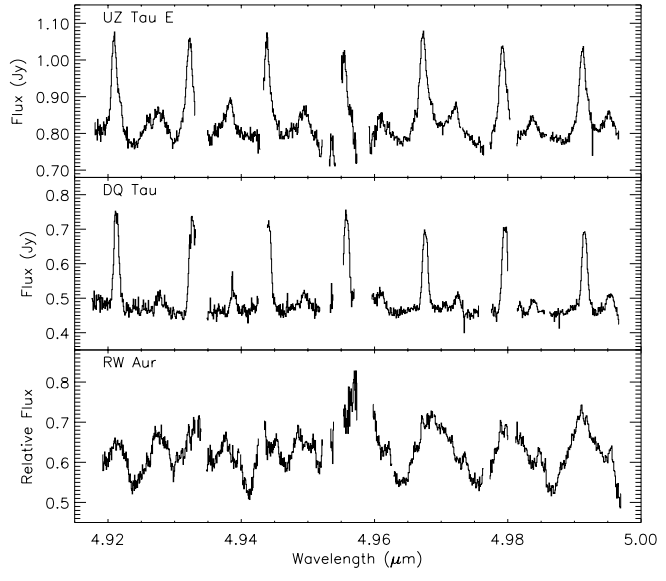

FIG. 2*f*

at the sensitivity of our measurements. The frequent detection of 2–1 emission indicates that at least some of the emission comes from warm gas ($\gtrsim$1000 K). At these temperatures, the CO $v = 3$–2 (hereafter 3–2) lines are expected to be significantly weaker than the CO 2–1 lines. CO 3–2 emission was clearly detected only from DF Tau and DQ Tau. We also detected ^{13}CO 1–0 emission from DF Tau (Fig. 2*g*). The ability to detect transitions

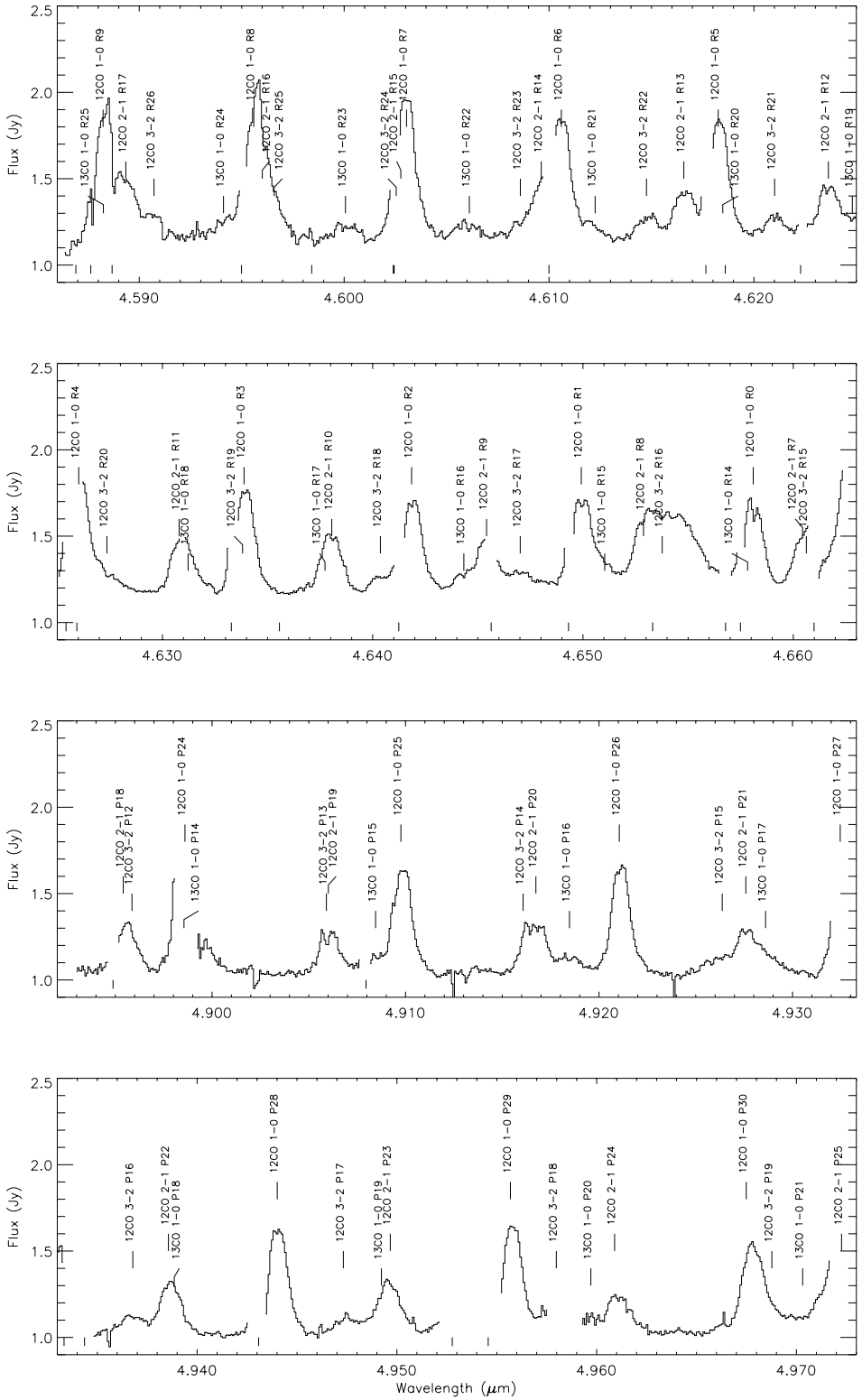

FIG. 2*g*

simultaneously from multiple isotopes and over a range of excitation conditions indicates the utility of CO fundamental emission for the measurement of circumstellar gas temperatures and column densities.

Apart from sensitivity considerations, the detection of weak lines, such as CO 3–2 and ^{13}CO, is also hampered by the blending of these lines with other lines of CO and potentially other molecular species. The DF Tau spectrum (Fig. 2*g*) shows the density of CO lines and the degree of blending that is evident in high-S/N spectra.

The RW Aur spectrum is a good example of an extreme case of blending. The features in the spectrum roughly correlate with those seen in the spectra of other sources (e.g., the UZ Tau E spectrum), although the lines

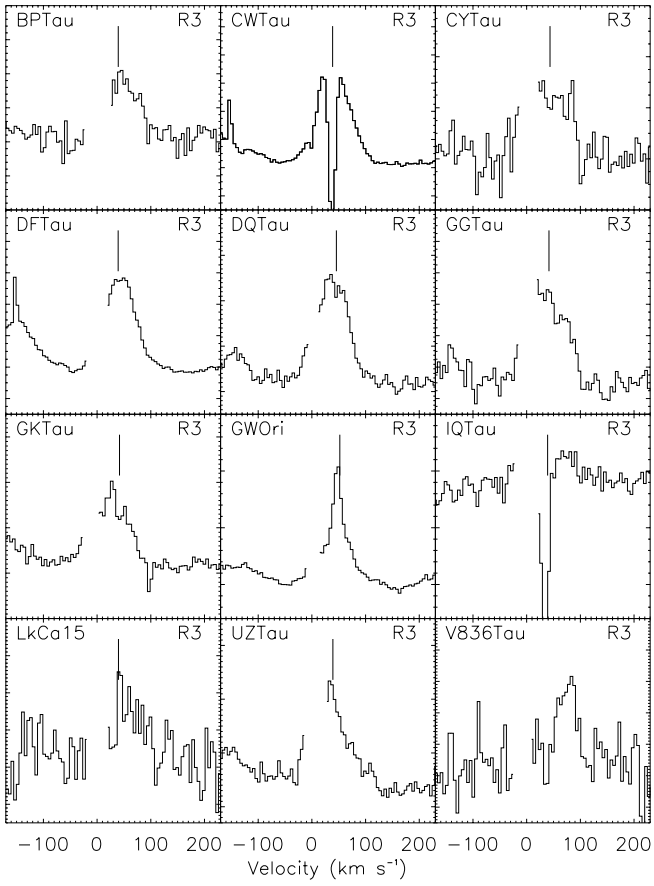

FIG. 3*a*

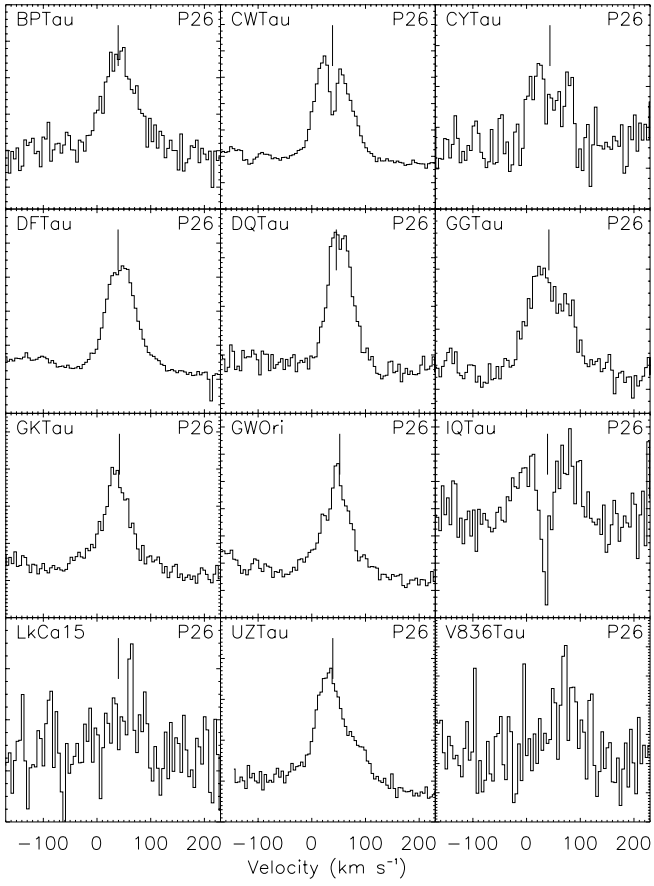

FIG. 3*b*

FIG. 3.—(*a*) CO 1–0 *R*(3) and (*b*) CO 1–0 *P*(26) line profiles of the sources observed with NIRSPEC. In each panel, the vertical line shows the predicted radial velocity of the source.

appear to be much broader. In addition, the 2–1 lines appear to be comparable in strength to the 1–0 lines, suggesting that the emission originates from much hotter gas. In § 5.1 we use simple spectrum synthesis modeling to illustrate these points.

To illustrate better the CO line profiles, Figure 3 shows an enlargement of the spectral region around the 1–0 *R*(3) and 1–0 *P*(26) lines for each source in which CO emission was detected with NIRSPEC. (The one exception is the spectrum of RW Aur, which has broad, highly blended emission lines and is therefore not shown.) Since the 1–0 *R*(3) and 1–0 *P*(26) lines experience relatively little blending with other CO lines, the profiles shown in Figures 1 and 3 should provide a reasonable representation of the profiles of individual lines. In general, the line profiles are broad (typical FWHM $\simeq 70$ km s^{-1}; see Tables 4 and 5) and fairly symmetric. Departures from this first-order characterization are more readily evident in the sources with higher S/N spectra. For example, in the NIRSPEC data, the GG Tau and UZ Tau E profiles are noticeably asymmetric, with stronger emission on the blue side of the line profile compared to the red. The GW Ori and GK Tau profiles have significantly broader wings compared to a Gaussian. The CY Tau profiles are flat-topped (the DF Tau and DQ Tau profiles are also flat-topped, but less so), as might be expected for disk emission originating from a range of velocities. In general, the profiles are not strongly double-peaked, as would be produced from a narrow annulus of emitting disk gas.

Some of the sources show narrow central reversals in their 1–0 emission-line profiles (CW Tau, IQ Tau, DQ Tau, and GK Tau). The weaker central reversals in the DQ Tau and GK Tau profiles are best illustrated in the 1–0 *R*(1) and *R*(2) lines. These features may indicate rotational velocity structure or may result from absorption at the systemic velocity. Several clues favor the latter interpretation. The reversals are detected in sources with higher A_V (Table 1), and the strongest reversals (CW Tau and IQ Tau) dip below the continuum, similar to the absorption features found in the RY

TABLE 4
CSHELL EMISSION-LINE PROPERTIES

Source	CO Line	FWHM (km s^{-1})	Flux (10^{-17} W m^{-2})
CW Tau	1–0 *R*(3)	45 ± 20	5.6 ± 1.1
DF Tau	1–0 *R*(3)	74 ± 10	6.3 ± 0.7
DQ Tau	1–0 *R*(3) 1995	54 ± 6	...
	1–0 *R*(3) 1996	69 ± 8	2.8 ± 0.2
	1–0 *R*(3) 1998	58 ± 6	3.6 ± 0.2
	1–0 *P*(18)	68 ± 4	6.9 ± 0.3
GW Ori	1–0 *R*(3) 1995	25 ± 5	...
	1–0 *R*(3) 1996	16 ± 4	5.0 ± 0.3
	1–0 *R*(6)	30 ± 3	12.7 ± 0.6
	1–0 *P*(18)	16 ± 4	11.5 ± 0.6
UZ Tau E	1–0 *R*(3)	85 ± 10	4.0 ± 0.7

TABLE 5
NIRSPEC Emission-Line Widths (FWHM)

Source	$\sigma_{1-0\,R}$ (km s^{-1})	$\sigma_{1-0\,P}$ (km s^{-1})	σ_{2-1} (km s^{-1})	σ_{3-2} (km s^{-1})
BP Tau	65 ± 4	70 ± 3	56 ± 22	...
CW Tau	72 ± 6	72 ± 6	99 ± 23	...
CY Tau	75 ± 11	86 ± 9	74 ± 18	...
DF Tau	73 ± 5	65 ± 5	78 ± 13	76 ± 18
DQ Tau	65 ± 7	57 ± 6	72 ± 16	59 ± 25
GG Tau	95 ± 14	93 ± 15	120 ± 22	...
GK Tau	64 ± 4	71 ± 6	91 ± 21	...
GW Ori	46 ± 6	72 ± 6	134 ± 30	...
UZ Tau	79 ± 11	87 ± 13	107 ± 25	64 ± 10
IQ Tau	...[a]	102 ± 10	...	...
LkCa 15	...[a]	82 ± 23	...	...
V836 Tau	41 ± 10	58 ± 14	...	...

[a] Uncertain because of telluric (and, in the case of IQ Tau, interstellar) absorption.

TABLE 6
NIRSPEC Line Fluxes and Temperatures

Source	F(1–0 $R3$) (10^{-17} W m^{-2})	F(1–0 $P26$) (10^{-17} W m^{-2})	T_{ex}(thin)[a] (K)
BP Tau	1.3 ± 0.2	1.9 ± 0.2	1158 ± 38
CW Tau	$11. \pm 1.2$	$14. \pm 1.4$	1385 ± 21
CY Tau	0.6 ± 0.2	0.5 ± 0.1	1297 ± 93
DF Tau	7.9 ± 1.0	8.1 ± 1.0	1814 ± 40
DQ Tau	4.0 ± 0.4	3.0 ± 0.4	1274 ± 30
GG Tau	1.1 ± 0.1	1.7 ± 0.1	1355 ± 57
GK Tau	2.2 ± 0.3	3.6 ± 0.4	1337 ± 39
GW Ori	8.3 ± 1.4	$10. \pm 1.0$	3222 ± 167
UZ Tau	2.6 ± 0.2	4.4 ± 0.4	1578 ± 47
IQ Tau	...[b]	1.3 ± 0.2	...
LkCa 15	...[b]	0.4 ± 0.1	...
V836 Tau	0.2 ± 0.1	0.3 ± 0.1	...

[a] Excitation temperature determined assuming that the emission is optically thin (see § 4.2.2).
[b] Uncertain because of telluric (and, in the case of IQ Tau, interstellar) absorption.

Tau and DG Tau spectra obtained with CSHELL. In addition, the strength of the reversal varies systematically for the different lines. If each line is fitted as a combination of an emission and an absorption component (see § 4), the absorption components are often fitted with a much lower temperature than the emission components. These features seem difficult to explain as a consequence of rotation. Assuming that the central reversals are absorption features, they may mask an underlying double-peaked profile that is due to rotation.

The line profiles also appear to be variable. Figure 4 compares the CSHELL and NIRSPEC profiles taken at different epochs. Whereas the GW Ori and DQ Tau profiles show little change between the two epochs, the UZ Tau E profile is much more peaked in the NIRSPEC data. The CW Tau profile is very asymmetric in the CSHELL data (weaker on the red side of the profile) but quite symmetric in the NIRSPEC data.

4. ANALYSIS

4.1. *Profile Fitting*

To give a preliminary characterization of the CO emission from our NIRSPEC sample, we used Gaussian lines to fit the spectra showing strong emission. (Excluded from this analysis is the highly blended spectrum of RW Aur, which is considered separately in § 5.1.) Compared to this simple analysis, considerably more information can be obtained by using spectral synthesis to characterize the emission at each disk radius, a more detailed analysis that will be reported in future publications. For the simpler characterization reported here, the lines chosen for fitting were typically those with the least blending with other CO emission features and those least compromised by strong telluric absorption. The spectra were fitted with a Marquardt routine using Gaussian line profiles and a second-order polynomial fit to the continuum. Each line was fitted with a single Gaussian emission component, where the amplitude, width, and line-center position were, in general, treated as free parameters. For some of the weaker lines, the position of the line was held fixed at the radial velocity of the star. Additional Gaussian *absorption* components were used to fit some of the sources. Regions of strong telluric absorption were excluded from the fit, with equal weighting assumed for the rest of the spectrum.

This characterization seemed adequate to estimate the fluxes, widths, and velocity centroids of the lines. The line widths and strengths determined from these fits are shown in Tables 5 and 6 and are discussed in more detail below. The Marquardt routine produces its own estimate of the 1 σ error in the fit, but the fitting does not take into account other factors that may contribute to the true error in the measured line parameters: residual errors in the correction of telluric absorption features, possible emission from very weak lines of CO or other unidentified molecules (e.g., H_2O), or residual spectral fringing. These factors will primarily affect the measured fluxes and widths of the weaker

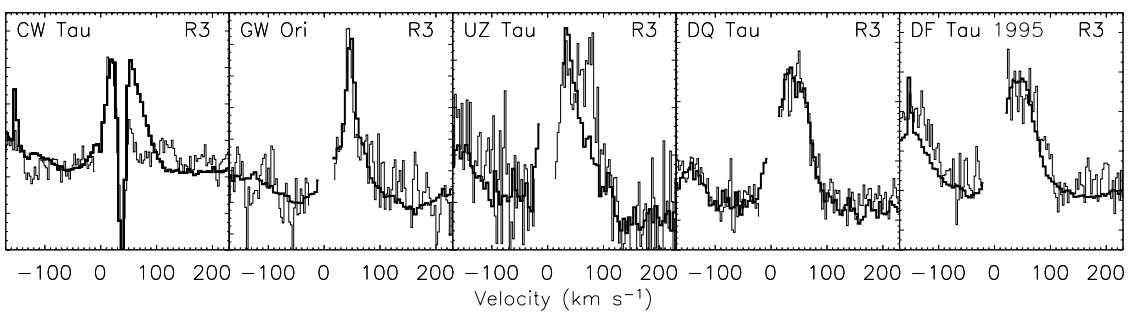

Fig. 4.—Comparison of the CO 1–0 $R(3)$ profiles measured with NIRSPEC (*thick lines*) and CSHELL (*thin lines*)

2–1 and 3–2 CO lines. Of the 1–0 lines we observed, the cleanest line was the 1–0 $P(26)$ line. Hence, this line is often used in the analysis and discussion in § 5.

4.2. *Emission Components*

4.2.1. *Line-Center Velocities and Widths*

The fitted line-center velocities are generally consistent with emission centered on the radial velocity of the star, although the line profiles are often not completely symmetric. Table 5 shows the average fitted line width (FWHM) for the 1–0 R, 1–0 P, 2–1, and 3–2 lines for the NIRSPEC sources. These can be compared with the measured line widths (FWHM) shown in Table 4 for the 1–0 lines observed with CSHELL. The line widths in the two tables are generally in agreement. However, some noticeable differences result from the different ways in which the line widths were measured in the two tables (e.g., GW Ori) as well as from actual apparent variability in the line profile (e.g., CW Tau). The errors cited in Table 5 are the standard deviations of the fitted line widths. The dispersion for the 1–0 R and 1–0 P lines was consistent with the errors estimated in the fitting process. In some of the sources, the 2–1 lines showed a greater dispersion in their widths than was consistent with the estimated errors. This is likely due to the difficulties associated with measuring weak lines (§ 4.1).

The FWHM of the 1–0 lines is typically $\sim$70 km s^{-1}. The widths of the 2–1 lines are equal to or greater than the 1–0 lines, but the lower S/N of, and greater scatter in, the 2–1 line widths often make the comparison difficult. The 2–1 lines are clearly broader than the 1–0 lines in three stars, CW Tau, GW Ori, and UZ Tau E, and they are marginally broader in GK Tau. There appears to be little statistically significant difference between the average widths of the 1–0 R and 1–0 P lines. One exception is GW Ori, where the line profile has both a narrow and a broad component, and there is a real trend of increasing line widths from the 1–0 R, to 1–0 P, to 2–1 lines. The narrow component is very prominent in the 1–0 R lines, less prominent in the 1–0 P lines, and absent in the 2–1 lines (see Figs. 1*c*, 2*c*, 2*d*, and 3). This suggests that the narrow component arises from cooler gas than the broad component, the situation that is expected for an origin in a disk with an outwardly decreasing temperature profile.

4.2.2. *Line Fluxes and Excitation Temperature*

Table 6 lists the fluxes measured for two representative lines, 1–0 $R(3)$ and 1–0 $P(26)$, in the NIRSPEC data. The fluxes and errors quoted in the table are the values estimated in the fitting process. A comparison of these values with the line fluxes measured with CSHELL (Table 4) shows that the CO emission flux often varies significantly with time. As previously noted (§ 3; Fig. 4), the line profiles can also change with time.

We can use the fluxes of the CO emission lines present in the NIRSPEC spectra to estimate the excitation temperature. (Excluded from this analysis are the low-S/N spectra of IQ Tau, LkCa 15, and V836 Tau and the highly blended spectrum of RW Aur. The excitation temperature of the emission from RW Aur is investigated in § 5.1 using spectral synthesis modeling.) In Figure 5, we plot $X_e = \ln(F/\nu g_u A_{ul})$ against E_u, where F is the measured line flux, ν is the wavenumber of the transition, g_u is the multiplicity of the upper level, A_{ul} is the A-value of the transition, and E_u is the energy of the upper level. If the CO emission is optically thin and the energy levels are thermally populated, $X_e \propto \exp(-E_u/kT_e)$, so $d(\ln X_e)/dE_u = -1/kT_e$, and the excitation temperature can be obtained from the slope in the plot. (Of course, it is likely that gas over a range of temperatures contributes to the line profile and flux, so that fits that derive a single temperature from integrated line fluxes actually represent some average excitation temperature for the emitting gas.) With these same assumptions, we previously estimated the excitation temperature for the CO fundamental emission from DQ Tau using the fluxes of four lines measured with CSHELL (Carr et al. 2001). With the larger number of lines observed simultaneously in the NIRSPEC data, we can examine the CO excitation more closely and determine whether the optically thin assumption is valid. The excitation temperatures obtained from the optically thin fits are listed in Table 6.

Examination of the plots in Figure 5 shows that the points do deviate from a straight line for many of the stars. The relatively constant slope for DQ Tau and UZ Tau E suggests that the optical depths are modest. For DF Tau, the situation is unclear because we were able to measure only a small number of relatively unblended lines because of the richness of its CO emission spectrum. However, the ready detection of ^{13}CO emission from DF Tau indicates that the ^{12}CO emission must be optically thick. For the other sources with well-measured lines, we often find a common pattern in the deviation of the points from a straight line: the low-J 1–0 R lines have a steeper slope, and the high-J 1–0 P lines a flatter slope (see, in particular, the plots for CW Tau, GW Ori, GK Tau, and GG Tau). This is the pattern expected from gas with moderate to large optical depth.

To illustrate this, Figure 6*a* shows the excitation plot for CW Tau where we have overplotted the values that would be produced by gas in LTE with an excitation temperature of 800 K and a column density of $\Sigma = 0.01$ g cm^{-2} (*plus signs*). The intrinsic line profile is assumed to be Gaussian with a thermal width, and an arbitrary constant has been added for comparison with the measurements. These parameters produce a reasonable "by-eye" fit to the measured values. At this column density, the line-center optical depths of the 1–0 $R(3)$, 1–0 $P(26)$, and 2–1 $P(18)$ lines are 7, 6, and 0.6, respectively, and only the high-J 2–1 lines are optically thin enough to obtain the correct excitation temperature directly from the slope. As a result, a fit to the fluxes of all of the measured lines (Fig. 5; $T_{\rm ex} \simeq 1390$ K), where it is assumed that all of the lines are optically thin, produces a significantly larger estimate of the excitation temperature.

Unfortunately, the scatter in the measured fluxes for the 2–1 lines is too large to constrain the temperature from their slope. Given the large optical depths in the 1–0 lines and the uncertainty in the fluxes of the 2–1 lines, significantly different temperature and column density combinations can produce equally good fits. For example, an excitation temperature of 600 K and $\Sigma = 0.03$ g cm^{-2} provides an equally good fit. With these parameters, the line-center optical depths of the 1–0 $R(3)$, 1–0 $P(26)$, and 2–1 $P(18)$ lines are 68, 24, and 1, respectively. In this case, the 1–0 $R(3)$ and $P(26)$ lines are again optically thick but at much higher optical depths, whereas the 2–1 $P(18)$ line has a comparable optical depth to that in the 800 K fit.

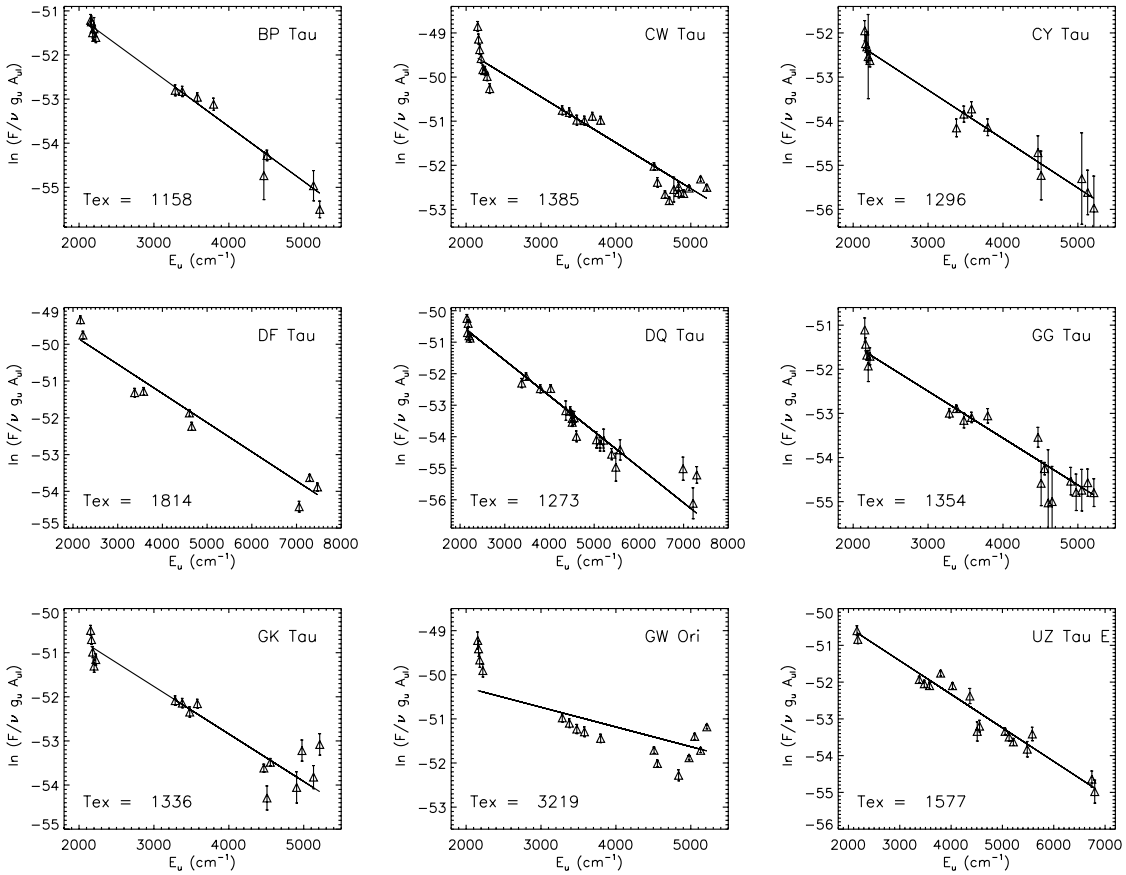

FIG. 5.—Estimated excitation temperatures for the NIRSPEC sources assuming optically thin emission. The quantity $\ln(F/\nu g_u A_{ul})$ is plotted against E_u, the energy of the upper level, where F is the fitted line flux (in W m^{-2}), ν is the wavenumber of the transition (in cm^{-1}), g_u is the multiplicity of the upper level, and A_{ul} is the A-value of the transition (in s^{-1}). The solid lines show fits to the measured values (*triangles*). The corresponding excitation temperature is given in the lower left corner of each plot.

Our by-eye fits for the other NIRSPEC sources, where optical depth is included as a parameter, find temperatures ranging from ~1500 K for UZ Tau E to more typical temperatures of ~1100–1300 K for most of the sources, to fairly cool (<1000 K) temperatures for CW Tau. Thus, when the optical depths are modest, the resulting temperatures are 200–300 K cooler than the optically thin temperatures, but the estimated temperature may be significantly cooler if the optical depths are large.

Another potential explanation for the nonlinear pattern in the excitation plots is the possibility of UV pumping (e.g., Krotkov, Wang, & Scoville 1980), where cold gas that is excited by UV photons produces more emission (especially from higher energy levels) than can be produced by thermal excitation alone. UV pumping has been suggested to play a

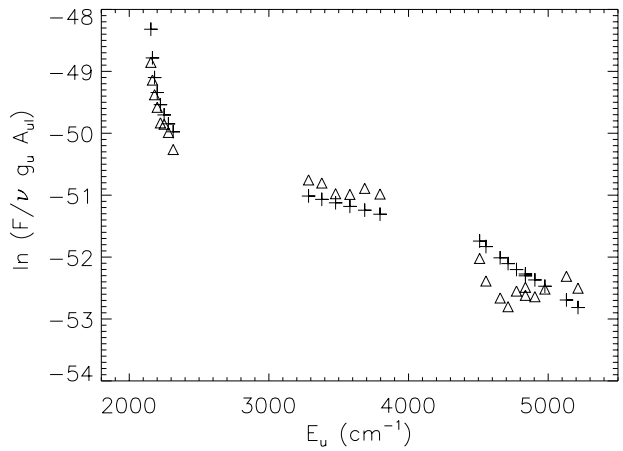

FIG. 6*a*

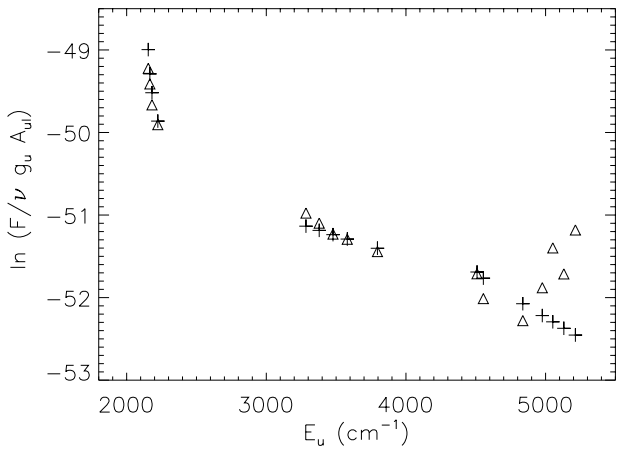

FIG. 6*b*

FIG. 6.—(*a*) Example of a possible optically thick fit (*plus signs*) to the line fluxes for CW Tau (*triangles*). The parameters of the fit are a temperature of 800 K and a column density of 0.01 g cm^{-2}. Because of the scatter in the fluxes of the 2–1 lines, other parameters (e.g., 600 K and 0.03 g cm^{-2}) will produce an equally good fit. (*b*) A possible optically thick fit (*plus signs*) to the line fluxes for GW Ori (*triangles*). The parameters of the fit are a temperature of 1100 K and a column density of 0.007 g cm^{-2}, but an equally good fit would be obtained with 700 K and 0.04 g cm^{-2}.

role in explaining CO fundamental emission from the Herbig AeBe star HD 141569 (Brittain & Rettig 2002). In this source, the relative fluxes of the low-J 1–0 lines suggest a gas temperature of $\sim$200 K, whereas the neighboring low-J 2–1 lines are much brighter than would be produced by gas at such a low temperature. This is similar to the situation seen in our data (e.g., the low-J 1–0 lines alone give 190 K for CW Tau), but UV pumping is less likely to be relevant here. For one, T Tauri stars are much weaker sources of UV flux than are Herbig AeBe stars. More importantly, we detect strong emission from the high-J 1–0 P lines. Since the selection rules require $|\Delta J| \leq 1$, it is difficult for UV photons to pump the low-J levels populated by cold $\lesssim$200 K gas to produce vibrational emission from $J \simeq 30$ levels. In other words, the excitation temperature required to populate the rotational ladder is also sufficient to produce the observed vibrational excitation.

A more plausible, alternative explanation for the nonlinear pattern in the excitation plots is the possibility of multiple temperature components, i.e., that the steep slope of the 1–0 R lines and the shallow slope of the 1–0 P lines arise from gas at two different temperatures. This seems unlikely to explain the results for most of the sources. For example, separate linear fits to the low-J R-branch lines and the higher-J P-branch lines in CW Tau give temperatures of 190 and 3800 K, respectively. It seems highly unlikely that two sets of lines with such vastly different temperatures would have line profiles that are indistinguishable. Similarly discrepant temperatures are implied by the slopes of the 1–0 R and P lines for GG Tau, GK Tau, GW Ori, and BP Tau.

GW Ori is a notable exception in this regard. Of the stars in our sample, only GW Ori shows a noticeable change in the line profile shape as a function of upper energy level. The optically thin fit for this source is particularly poor (Fig. 5), and a significantly lower temperature is implied by an optically thick fit (Table 6; Fig. 6*b*). While the optically thick fit works well for the low- and high-J lines, given the two-component structure of the GW Ori line profiles, it is quite possible that two temperature components contribute to the extreme shape of the excitation plot. Detailed modeling of the line profiles can be used to determine the extent to which multiple temperature components and optical depth are needed to reproduce the observed line profiles and fluxes.

Thus, we conclude that the CO fundamental emission is mainly thermally excited, but great care is required in order to derive accurate gas temperatures and masses from the emission. Because relatively small column densities ($>$0.001 g cm^{-2}) can produce modest to high optical depths in the 1–0 lines, the assumption of optically thin emission can lead to invalid results, particularly if the observed lines are small in number or cover a limited range in excitation potential. For example, if only the low-J 1–0 lines were observed, then erroneously low temperatures would be derived (e.g., $\sim$200 K in CW Tau), when in fact the emission is optically thick from gas at much higher temperatures. Similarly, if only high-J 1–0 lines were observed, then mistakenly high temperatures would be derived (e.g., $\sim$4000 K in CW Tau).

4.3. *Absorption Components*

CO absorption components are observed in the spectra of CW Tau, DQ Tau, GK Tau, IQ Tau, RY Tau, and DG Tau. In all cases, the absorption components are spectrally unresolved. For the four sources in which absorption was detected in multiple transitions, the excitation temperature of the absorbing gas T_a can be obtained from $d(\ln X_a)/dE_l = -1/kT_a$, where $X_a = -F\nu^2/g_u A_{ul}$, under the assumption that the absorption is optically thin and the energy levels are thermally populated. In these expressions, F is the flux in the absorption feature, and E_l is the energy of the lower level. We find estimated excitation temperatures of 930 ± 120, 7 ± 2, 17 ± 10, and 1200 ± 200 K for the absorbing gas in CW Tau, DQ Tau, GK Tau, and IQ Tau, respectively. In the IQ Tau spectrum, the absorption-line fluxes are comparable up to the high-J P transitions, which suggests that the absorption is optically thick. A similar situation is found for CW Tau. As a result, the temperatures estimated for these sources are probably not very accurate. Nevertheless, the absorbing gas in these two systems must be fairly warm in order to populate the high-J levels from which absorption is observed.

The low absorption temperatures measured for DQ Tau and GK Tau are consistent with an origin in cold gas not in the immediate vicinity of the star, e.g., in the surrounding molecular cloud. The much higher absorption temperature inferred for CW Tau suggests that the absorbing gas is located much closer to the star. If the absorption occurs in the atmosphere of a (nearly edge-on) disk, it may be possible to produce a warm gaseous absorption feature without an overly large dust extinction along the line of sight. This may explain the absorption features in CW Tau, which has a high $v \sin i$ (27 km s^{-1}; Hartmann & Stauffer 1989) suggestive of a high inclination. However, it seems unlikely, statistically, that we would then have two nearly edge-on sources in our sample, and moreover, the rotation period and $v \sin i$ for IQ Tau are consistent with an intermediate inclination (see Table 8). Thus, the origin of the warm absorption features appears to be an open question.

5. DISCUSSION

5.1. *Comparison with* CO *Overtone Emission*

As described above, CO fundamental emission is found to be very common among T Tauri stars. This is in marked contrast to the situation found for CO overtone emission. Although the overtone bands are commonly detected in emission among energetic outflow sources ($\sim$20% show emission; Carr 1989), low spectral resolution surveys of star-forming regions find that overtone emission is much rarer among the general young stellar object population (a few percent show overtone emission; e.g., Greene & Lada 1996; Luhman & Rieke 1998). One could postulate that CO overtone emission is present but is usually missed at low spectral resolution because the equivalent width of CO absorption in T Tauri stellar atmospheres is comparable to or greater than the CO emission equivalent width. However, in a modest survey of T Tauri stars at a resolution high enough ($R \sim 20,000$) to separate narrow stellar absorption from higher velocity emission, J. S. Carr & J. R. Najita (1995, unpublished) found strong emission in only one of 15 sources not previously known to have emission. This supports the result of the larger low-resolution surveys: CO overtone band-head emission is not common among T Tauri stars.

The difference in the incidence rate of CO overtone and fundamental emission is probably due, in part, to the

smaller A-values of the overtone transitions, which are approximately 2 orders of magnitude smaller than those of the fundamental transitions. Using spectral synthesis modeling, Najita et al. (1996) found that large gas column densities ($\sim$0.1–1000 g cm^{-2}) are required to produce the strength and shape of the overtone emission. This contrasts with the far lower column densities, less than 0.1 g cm^{-2}, that generally characterize CO fundamental emission in T Tauri stars (§ 4.2.2). In addition, gas temperatures of $\geq$2500 K are required to produce the overtone emission that is observed from high vibrational and rotational upper levels (e.g., $v = 4$, $J = 50$), compared to the temperature of $\sim$1200 K that is typical of the CO fundamental emission in our sample. The larger temperature and column density conditions required to put the overtone bands into emission appear to be rarely met, since CO overtone emission is only observed from the most active T Tauri stars (e.g., DG Tau, RW Aur, AS 353A, and V1331 Cyg), i.e., stars with the largest optical veiling, Hα equivalent width, and infrared excess. On the other hand, the conditions required to produce CO fundamental emission appear to be common among T Tauri stars.

Of the 18 stars that we surveyed for CO fundamental emission, 11 have previous spectroscopy of the CO overtone bands at either low or high resolution (Carr 1989; Greene & Lada 1996; J. S. Carr & J. R. Najita 1995, unpublished). Of these, the two stars known to have prominent CO overtone band-head emission are RW Aur (J. S. Carr & J. R. Najita 1995, unpublished) and DG Tau (Hamann, Simon, & Ridgway 1988; Carr 1989). In the rest of this section, we use simple spectral synthesis modeling (see Najita et al. 1996; Carr et al. 2001) to demonstrate that, for these overtone-emitting sources, the fundamental emission likely originates from the same (disk) gas. The origin of the fundamental emission from the rest of the sample is discussed in § 5.2.

The CO fundamental emission spectrum of RW Aur appears substantially different from those of the other emission sources (see Figs. 2*e* and 2*f*). The general appearance suggests larger velocity widths and additional (higher vibrational) emission lines. Figure 7 shows a portion of the RW Aur spectrum overplotted with a disk model that reasonably matches the observed spectrum. In the model, the assumed temperature, rotational velocity, and column density at the inner emission radius $R_{\rm in}$ are $T = 3500$ K, $v \sin i = 250$ km s^{-1}, and $\sigma = 0.1$ g cm^{-2}, respectively. The temperature and column density decrease as $\propto r^{-0.3}$, and the outer radius for the emission $R_{\rm out} \simeq 10 R_{\rm in}$, or $v \sin i = 80$ km s^{-1}. Substantial emission is produced from the higher vibrational levels $v = 3$ and 4. The CO line fluxes from RW Aur are among the strongest in the sample. For example, in comparison to the line fluxes in Table 6, the blended 1–0 $P(26)$ feature in the RW Aur spectrum has a flux of 20×10^{-17} W m^{-2}, while our model predicts a flux of 13×10^{-17} W m^{-2} for the $P(26)$ line.

Since the emission is very optically thick, e.g., $\tau \sim 40$ in the 1–0 $P(26)$ line, the spectrum is insensitive to the excitation temperature. For example, an equally good fit is obtained if the column density and temperature are instead constant, with $T = 3500$–1500 K, and all other parameters are unchanged. However, temperatures lower than these fail to match both the shape of the spectrum and the total line flux, and hot ($\sim$3500 K), less optically thick models ($\tau \lesssim 1$) can fit the spectral shape but not the flux. This confirms the expectation from Figure 2 that the gas conditions characteristic of the other CO fundamental emission sources ($T \sim 1500$ K and low to moderate optical depths) cannot explain the RW Aur spectrum. The large velocity dispersion, warm temperatures, and high optical depths required to reproduce the RW Aur spectrum are reminiscent of the conditions required for overtone band-head emission. Indeed, if the fundamental and overtone from RW Aur are produced by the same gas, we can further constrain the properties of the emission to be optically thick at $T \sim 3500$ K.

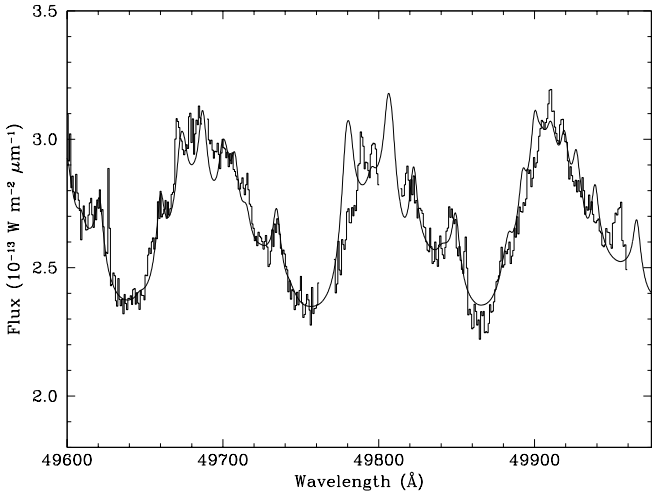

FIG. 7.—Comparison of a portion of the RW Aur CO spectrum (*histogram*) with a disk emission model (*solid line*). A double-peaked line profile is required to fit the observed spectral shape. The strength and shape of the CO fundamental and overtone spectra are consistent with optically thick emission from warm (>1500 K) gas. See § 5.1 for details.

A particularly interesting result is that for RW Aur, unlike the majority of fundamental emission sources, a double-peaked disk profile is required to fit the observed spectrum (Fig. 7; e.g., the sharp features at 4.9660 and 4.9735 μm). Thus, the emission must cut off fairly sharply at its outer radius. The spectrum places fairly good constraints on $v \sin i$ of 250 and 80 km s^{-1} at $R_{\rm in}$ and $R_{\rm out}$, respectively. Assuming a stellar mass of 1.3 $M_\odot$ and inclination $i = 60°$, these velocities correspond to disk radii of 3–30 $R_\odot$, which would place the inner edge of the emitting gas within $2R_*$.

In the spectrum of DG Tau (Fig. 1*b*), centered on the 1–0 $R(3)$ line, CO emission is not obvious. Variability is an issue in this case, because the CO overtone emission from DG Tau is known to be variable, sometimes disappearing at low spectral resolution (Greene & Lada 1996; Biscaya et al. 1997; J. S. Carr, J. R. Najita, & A. T. Tokunaga 2001, unpublished data). However, we obtained a high-resolution CSHELL spectrum of the CO $v = 2$–0 band-head emission from DG Tau on the same night that we observed the 4.63 μm spectrum, and the overtone band head is strongly in emission. Therefore, CO fundamental emission should be present. Indeed, the 4.63 μm spectrum shows structure that could be produced by broad disk emission.

Figure 8 shows the DG Tau spectrum overplotted with a disk model that reasonably matches the observed spectral structure. The parameters of the model are nearly identical to those for RW Aur. The main differences are the inner $v \sin i = 200$ km s^{-1} and a larger column density at the inner

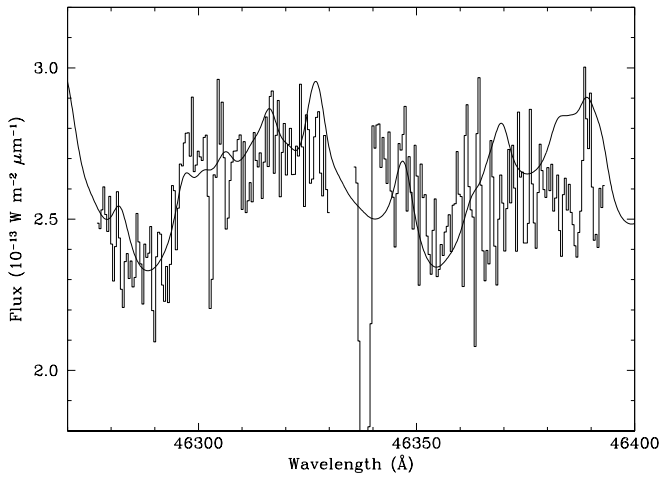

FIG. 8.—Comparison of the DG Tau spectrum obtained with CSHELL centered on the $v = 1$–0 $R(3)$ line (*histogram*) with a possible synthetic disk emission spectrum (*solid line*). Apart from the narrow central absorption feature, which is probably interstellar (see § 4.3), the observed spectral structure is consistent with broad CO emission. See § 5.1 for details.

edge, $\sigma = 0.5$ g cm^{-2}. In the model spectrum, the flux of the $R(3)$ line alone is large, 8×10^{-17} W m^{-2}, comparable in strength to the emission from DF Tau and GW Ori. The modeling shows the plausible presence of strong CO fundamental emission in DG Tau, which is otherwise less than obvious because of the limited spectral coverage, large line widths, and the dilution by continuum emission. While these data are not sufficient to constrain the gas parameters, they are consistent with optically thick emission from hot gas similar to that observed in RW Aur.

Thus, in the two stars known to have CO overtone emission, CO fundamental emission is present, but the velocity dispersion and temperature of the emitting gas are both substantially higher than is found for the other CO fundamental emission sources. Since the gas temperatures and velocities are consistent with the values required for CO overtone emission, it is highly likely that the CO fundamental and overtone emission are produced by the same gas.

5.2. *Origin of the Emission*

For the rest of the sample (i.e., sources without overtone emission), we can attempt to diagnose the region of the young stellar environment that is responsible for the emission based on the demographics of the emission sources, the line profile shapes, and the emission temperatures estimated in § 4. CO fundamental emission is found to be correlated with various measures of accretion activity, a result that suggests an origin in either the wind, the funnel flow, or the disk. Of these, a disk origin is strongly favored by the CO line profile shapes and the emission temperatures. The evidence and arguments supporting this conclusion are discussed in greater detail in the rest of this section.

5.2.1. *Comparison with Accretion Indicators*

We find that the stars with the strongest CO fundamental emission are generally the most active T Tauri stars in our sample, while the stars with weak or no emission are the least active. For a more quantitative examination of this result, we compared the measured CO flux with two indicators of accretion activity: the $K-L$ color, which is a measure of the excess infrared emission from the disk, and the accretion rate as determined by veiling in the blue and ultraviolet, which is a measure of current accretion onto the stellar surface. The accretion rate is plotted against observed $K-L$ color in Figure 9 for the stars in the NIRSPEC sample. Stars without detected CO emission are shown as open symbols, and stars with detected emission are shown as filled symbols, where a larger symbol size indicates a larger flux in the 1–0 $P(26)$ line. The three spectroscopic binaries in our sample are plotted as squares.

In Figure 9, the $K-L$ colors are from the compilation of Kenyon & Hartmann (1995), except for GW Ori, which is from Mathieu, Adams, & Latham (1991). The accretion rates are from Gullbring et al. (1998, 2000), Valenti, Basri, & Johns (1993), Hartigan, Edwards, & Ghandour (1995), and Hartmann et al. (1998). While most of these papers determine the accretion rate based on the measured veiling in the blue and ultraviolet, their assumptions and procedures differ. Where multiple estimates were available, we preferred the values reported by Gullbring et al., followed by those of Valenti et al. When the estimates agreed to within a factor of 2, we averaged the estimates. One exception is DQ Tau, for which Gullbring et al. measured a negligible veiling and a correspondingly small accretion rate. Since the veiling in DQ Tau is known to be highly variable (Basri, Johns-Krull, & Mathieu 1997), their spectrum must have sampled a period of unusually low accretion; hence, we adopted the higher accretion rate derived by Valenti et al. for this source. Accretion rates from Hartigan et al. were adopted for two stars: V836 Tau, which was not analyzed in the other papers, and CW Tau, for which Valenti et al. found an unusually low accretion rate for this extremely active T Tauri star. The Hartigan et al. accretion rates were multiplied by 0.07, as recommended by Gullbring et al., in order to bring the Hartigan et al. rates onto the same average scale.

Figure 9 shows that the mass accretion rate is correlated with the $K-L$ color. This is similar to other results for T Tauri stars in general, e.g., the correlation between veiling

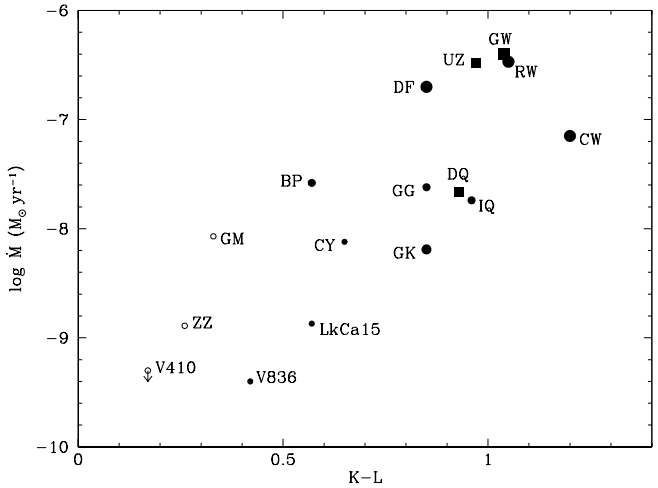

FIG. 9.—Comparison of the accretion rate and $K-L$ color for the NIRSPEC sources. Stars without detected CO emission are shown as open symbols. For the sources with detected emission (*filled symbols*), a larger symbol size indicates a larger flux in the CO 1–0 $P(26)$ line. The spectroscopic binaries are plotted as squares.

and infrared excess (Hartigan et al. 1990, 1995; Basri & Batalha 1990). Figure 9 also shows that the strength and presence of CO fundamental emission is related to these indicators of accretion. The stars with nondetections have the smallest accretion rates and $K-L$ colors; one of these, V410 Tau, is a weak T Tauri star. Among the stars with detected emission, those with the smallest CO line fluxes have smaller accretion rates and infrared excesses, while the stars with the largest accretion rates and infrared colors show the strongest CO emission. The CO emission temperature (see Table 6 and the discussion in §§ 4.2 and 5.1) is also related to the mass accretion rate. The stars with the highest temperatures (UZ Tau, DF Tau, and RW Aur) fall near the top of the figure; i.e., they have the highest accretion rates. Our disk spectral synthesis modeling in § 5.1 indicates that DG Tau belongs in this group. For this star, the accretion rate is $5 \times 10^{-7}\ M_{\odot}\ \mathrm{yr}^{-1}$, $K-L = 1.68$, the flux of the 1–0 $R(3)$ line in the synthetic disk spectrum is comparable to that of DF Tau, and the temperature of the emitting gas in the model is ~3000 K. The other stars have estimated CO temperatures of ~1200 K. Thus, the correlation between the CO fundamental emission and the accretion indicators suggests that the phenomenon of CO fundamental emission is closely related to the disk accretion process.

5.2.2. *Line Profile and Temperature Considerations*

In principle, these correlations allow for an origin in either the disk, a wind, or magnetic accretion columns since these physical components are all believed to play roles in the accretion process. Of these alternatives, a wind seems the least likely. The CO emission-line profiles are mostly symmetric. Lines formed in outflowing gas are likely to have strongly asymmetric, P Cygni–like profiles with blueshifted absorption components, due to absorption by the wind of the disk and stellar continuum, and/or a global line asymmetry produced by the occultation of the receding flow by an optically thick inner disk. In contrast, we find that the line-center velocities for the CO fundamental lines are consistent with emission centered on the radial velocity of the star. In fact, the lack of blueshifted absorption, even in stars with strong and broad absorption in the Balmer and Na I lines (e.g., DG Tau and RW Aur), suggests that the winds do not possess a significant molecular component. Another argument against a wind origin for the emission is that some of the most energetic outflow sources show no CO fundamental emission (e.g., L1551 and SVS 13; J. S. Carr, J. R. Najita, & A. T. Tokunaga 1992, unpublished data), although these are the objects in which CO is most likely to form in a wind (Glassgold, Mamon, & Huggins 1991). It is possible that winds are too warm or too highly irradiated by X-rays for substantial CO to be maintained in a wind.

Magnetospheric accretion columns are another potential source for the CO emission. Hydrogen and many other permitted emission lines from T Tauri stars are currently believed to arise in a magnetospheric accretion flow (a funnel flow), where material flows from a truncated accretion disk onto the stellar surface (Hartmann, Hewett, & Calvet 1994; Edwards et al. 1994; Muzerolle, Calvet, & Hartmann 1998, 2001). The regions that produce the atomic line emission are certainly too hot to contain CO, but the outer regions of the accretion flow may be cool enough to possess a molecular component. The blue asymmetries seen in the CO profiles of some stars (UZ Tau, GG Tau, and CW Tau in 1997) may suggest that absorption from infalling gas is present, although as we discuss below, it seems very unlikely that the absorption occurs in a funnel flow.

This funnel flow scenario was considered by Martin (1997) for the origin of CO overtone emission in young stars. The model as presented by Martin is incomplete in two important respects. First, rotation is neglected: the gas is assumed to be in pure infall along the magnetic field lines. This is certainly not true in the outer regions of the funnel flow, where the gas leaving the disk has a large rotational component (e.g., Ostriker & Shu 1995). The second difficulty concerns the more general issue of the temperature structure in the accretion columns. Martin (1996) has made the only attempt, thus far, to calculate self-consistently the thermal structure of funnel flows. He found that adiabatic compression was the main heat source, giving maximum temperatures in the flow of ~6500 K. However, the mean temperatures derived are too low to produce the observed atomic line emission (Muzerolle et al. 1998, 2001), which suggests that an additional heating mechanism not considered by Martin is present (e.g., Alfvén-wave heating). In addition, an initial temperature of 3000 K was assumed for the gas entering the funnel flow; i.e., the thermal structure was not calculated at the radii and temperatures most conducive to CO fundamental emission.

Nevertheless, it seems unlikely that funnel flows are responsible for the bulk of the observed CO fundamental emission, based on both the required gas temperature and the observed line profiles. At the radii from which the funnel flows are believed to originate, disk temperatures are ~1000–1500 K (e.g., Shu et al. 1994). This should represent a minimum temperature for the material as it is loaded onto the field lines and begins to flow toward the star. If the gas is heated slowly enough that CO exists over some portion of the accretion column, it will emit until the temperature is high enough (~4000 K) to dissociate CO. Hence, we would expect the CO emission to be characterized by relatively high temperatures (1500–4000 K). With the exception of RW Aur, our data indicate mean temperatures of ~1200 K for the CO-emitting gas.

It also appears unlikely that CO in the outer regions of magnetic accretion columns would produce the type of line profiles that are observed. Gas in the funnel flow would initially have a large rotational component, equal to the local Keplerian velocity at the disk truncation radius. The calculation of Ostriker & Shu (1995) shows that the velocity field is dominated by the azimuthal component in the outer half of the flow and that the rotational velocity is roughly constant with radius. Gas with such a flat rotation curve, emitting over a relatively small range in radii, would produce a strongly double-peaked, steep-sided line profile. This is illustrated in Figure 10*a* by a simple model profile, where the emitting gas has a pure rotational profile that has a constant rotational velocity from the truncation radius of 9 $R_{\odot}$ down to 5 $R_{\odot}$. The maximum velocity in the model profile was chosen to match that in DF Tau, 80 km s^{-1}, a width that is typical of our sample. This is an advantageous characterization of the funnel flow since the poloidal infalling component of the flow, which would introduce any line asymmetry, is ignored. The 1–0 $P(26)$ line profile in DF Tau is shown in Figure 10*c*. With the possible exception of CY Tau, the centrally peaked profiles observed in our sample are very different from the model profile. Hence, infalling gas with dynamics similar to that calculated by Ostriker &

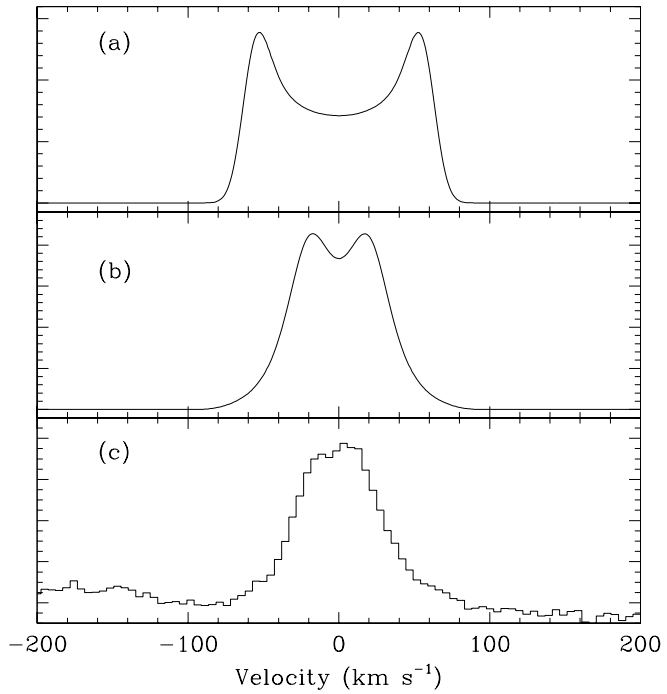

FIG. 10.—Comparison of idealized (*a*) funnel flow and (*b*) disk line profiles with (*c*) the CO emission profile of DF Tau, a profile that is typical of our sample. The funnel flow has been approximated as purely rotational with a velocity that is constant with radius, as appropriate for the outer half of the flow in which CO is likely to exist (see § 5.2.2 for details). The resulting double-peaked, steep-sided line profile is a poor match to the observed line profile, whereas the model line profile produced by disk emission over a range of radii (see § 5.2.2 for details) provides a reasonable match to the observed CO emission profile.

Shu (1995) cannot explain the observed CO fundamental profiles.

The third possibility, the inner accretion disk, is the strongest candidate for the source of the CO fundamental and overtone emission. In the case of the CO overtone band heads, a disk origin for the emission has been demonstrated fairly convincingly by previous high-resolution spectroscopy. Spectral synthesis modeling of the band heads reveals that the emission lines have the characteristic double-peaked spectral shape expected from gas in a rotating disk that is in emission over a limited range of radii (Carr et al. 1993; Chandler et al. 1995; Najita et al. 1996). In low-mass stars, this emission is found to originate from within ~0.2 AU of the star. In § 5.1 we showed that similarly double-peaked profiles are present in the RW Aur CO fundamental spectrum.

In contrast, double-peaked disk profiles are not obvious in the rest of the CO fundamental emission sample. (Again, CY Tau is a possible exception. The apparent double peaks seen in CW Tau and IQ Tau are likely due to narrow absorption lines from intervening gas.) A disk can produce the more centrally peaked profiles that are observed if the emission extends over a large range in radii. This is illustrated in Figure 10*b*, which shows a disk emission profile for the 1–0 $P(26)$ line. The $v \sin i$ at the inner disk emission radius is set at 80 km s^{-1}, as observed in DF Tau (Fig. 10*c*). The emission radius in the model ranges from 0.04 AU (a typical disk truncation radius; e.g., Shu et al. 1994) out to 1.6 AU, with an $r^{-0.4}$ temperature profile for the emitting gas. In this example, the CO temperature at the outer radius is 570 K.

To summarize, in an accretion disk scenario for CO rovibrational emission, the CO overtone band-head emission sources represent the extreme cases, in which the high-temperature, high column density conditions needed to excite the high vibrational and rotational levels are present in the innermost parts of the disk. Because the overtone band-head emission is dominated by hot gas over a narrow range of radii (as found in Najita et al. 1996), the profiles are more strongly doubled-peaked. In a more typical T Tauri star, the inner gas temperatures and emission column densities are not high enough to produce overtone band-head emission, but conditions are sufficient to populate the lower rotational levels of the ground and first excited vibrational levels. Because of the lower column densities required to put the fundamental lines into emission, the lower temperatures required to populate the $v = 1$ level, and the possibility of radiative trapping, emission from larger radii is possible. This results in narrower, more centrally peaked profiles and lower mean temperatures than in stars with overtone band-head emission. The high frequency of detection of CO fundamental emission, and the larger disk radii that it appears to probe, suggests its utility as an indicator of the presence of molecular gas in inner disks and as a tool with which to probe the kinematics and physical conditions of this region.

5.3. *Emission from Disk Atmospheres and Gaps*

Line emission from an accretion disk can arise in a variety of physical situations. Although the near-infrared excesses of T Tauri stars imply that T Tauri disks are generally optically thick, disks may have low continuum opacity regions of limited radial extent that are capable of producing line emission. For example, line emission may arise from hot gas within the dust destruction radius. This is essentially the model for CO overtone emission proposed by Carr (1989), although disk material may not be present at these radii if disks are truncated, as in the current magnetospheric accretion model for T Tauri stars. Optically thin regions in the form of gaps or inner holes may also be carved out by companion bodies, and regions of similarly low continuum optical depth may also arise as a consequence of grain growth. Alternatively, line emission from an optically thick disk can arise from temperature inversions in disk atmospheres, i.e., due to external heating.

We have previously argued that stars with close stellar or massive protoplanetary companions will show CO fundamental emission from residual low column density material within a dynamically cleared disk gap (Carr & Najita 1998; Najita et al. 2000; Carr et al. 2001). This is the interpretation we gave for the CO fundamental emission from the T Tauri spectroscopic binary system DQ Tau (Carr et al. 2001). There we found that the properties of the CO emission (the flux, temperature, and kinematics) could be explained by a small amount (10^{-5} $M_\oplus$) of material residing within 0.5 AU of the star, an extent that is close to the theoretically expected size for a dynamically cleared inner hole for this binary system. Dynamically cleared gaps are also expected in the accretion disks of the other two spectroscopic binaries in our sample, UZ Tau and GW Ori, both of which are found to show strong CO fundamental emission.

However, CO fundamental emission is not limited to these systems. Most of the apparently single stars and wider

binaries in our sample also show CO fundamental emission, and in fact, the spectroscopic binaries and the non–spectroscopic binary stars have similar CO emission properties.[1] The spectroscopic binaries are among the more active stars in the sample, but they are not otherwise unusual. Of the spectroscopic binaries, only GW Ori has a unique line profile, with narrow and broad components in the 1–0 lines. The CO line widths and profiles of DQ Tau and UZ Tau are similar to those of the non–spectroscopic binary stars. Unless most classical T Tauri stars have disk structure in the form of optically thin gaps or large inner holes, temperature inversions in disk atmospheres are required to explain the observed detection frequency. This raises two questions: are disk gaps really the source of CO emission in the spectroscopic binaries, and is the origin of the emission different for spectroscopic binaries and non–spectroscopic binary stars?

To address these questions, we can examine the line profiles of the spectroscopic binary and non–spectroscopic binary systems in order to estimate the radii from which the CO emission originates. Assuming Keplerian motion and that the stellar mass and the system inclination are known, the maximum velocity observed in the line wings directly gives the inner radius of the emission. Estimating the outer radius of the emission is more difficult, because the relation of the profile width to the Keplerian velocity at the outer radius depends on the radial intensity profile, which depends on the excitation conditions and the transition measured. Our modeling of disk profiles shows that for a flat radial intensity law, the half-width at half-maximum (HWHM) velocity corresponds to a radius of $\sim$0.5 times the outer emission radius, as long as the ratio of the outer and inner radii is greater than 8. This condition is likely met for our sample because the observed line profiles are not strongly double-peaked. For a more realistic line intensity law that decreases with radius, the outer radius associated with the HWHM velocity would be a few times larger. Hence, the former estimate based on the HWHM velocity gives a conservative *lower limit* to the outer emission radius.

5.3.1. *Spectroscopic Binaries*

We first examine the spectroscopic binaries. The periods and semimajor axes of the three spectroscopic binaries are listed in Table 7. In the same table, we also summarize the inner and outer radii (R_{in} and R_{out}) of the theoretically predicted extent of a disk gap in the system. These are compared with the inner and outer emission radii derived for the CO emission based on the line profile. As described above, the outer emission radius is expressed as a lower limit. The derivation of these quantities is described below for the individual binary systems.

For DQ Tau, the system parameters are a period of 15.8 days, an eccentricity of 0.56, an estimated total mass of 1.3 $M_\odot$ with a mass ratio close to 1.0, and a system inclination of 23° (Mathieu et al. 1997). The semimajor axis is 0.136 AU at this inclination. For these parameters, theory predicts a gap from 0.03 to 0.4 AU (Artymowicz & Lubow 1994). Taking the 1–0 $P(26)$ line as a representative profile, the maximum CO velocity is $\sim$59 km s^{-1} and the HWHM velocity is 26 km s^{-1}. This corresponds to an inner radius of 0.05 AU and an outer radius $\gtrsim$0.5 AU, which is consistent with our previous modeling of the line profile (Carr et al. 2001).

UZ Tau E is a system similar to DQ Tau; its orbit has a period of 19.1 days and an eccentricity of 0.28 (Mathieu, Martín, & Magazzu 1996), and the total mass is 1.3 $M_\odot$ (Simon, Dutrey, & Guilloteau 2000). However, UZ Tau E has a smaller mass ratio of 0.3 (Prato et al. 2002). Given the inclination of 54° (Prato et al. 2002), the semimajor axis is 0.16 AU. For this system, the results of Artymowicz & Lubow (1994) predict a disk gap of 0.05–0.4 AU. The 1–0 $P(26)$ line has a maximum velocity of 87 km s^{-1} and an FWHM of 71 km s^{-1}. However, the line profiles observed in 2001 are clearly asymmetric when the 1–0 $R(3)$ line is compared to the 1996 spectrum (Fig. 4). The 1996 1–0 $R(3)$ profile has a larger FWHM of 95 km s^{-1} but a similar maximum velocity in the wings. If we take the symmetric 1996 profile as being more representative of the underlying disk emission, then the inner CO radius is 0.1 AU and the outer radius is $\gtrsim$0.7 AU. Hence, the emission includes the radii predicted for the gap but may extend to larger radii.

The GW Ori system is a single-line spectroscopic binary with a period of 242 days, a nearly circular orbit, a primary-secondary separation of about 1.1 AU, and a primary mass of 2.5 $M_\odot$ (Mathieu et al. 1991). Modeling of the spectral energy distribution (SED) indicates a reduced column density of disk material over the range of radii 0.17–3.3 AU (Mathieu et al. 1991). The simulations of Artymowicz & Lubow (1994) predict a disk gap from 0.45 to about 2.0 AU.

[1] We group the spatially resolved binaries (DF Tau, GG Tau A, and GK Tau) with the single stars because the velocity widths of the CO fundamental lines are far too large to be associated with disk gaps at the projected separation of these systems (12, 35, and 340 AU, respectively).

TABLE 7
BINARY PARAMETERS AND CO EMISSION RADII

			Theoretical Gap		Emission Extent	
Star	P (days)	a (AU)	R_{in} (AU)	R_{out} (AU)	R_{in} (AU)	R_{out}(min)[a] (AU)
DQ Tau	15.8	0.136	0.03	0.40	0.05	0.5
UZ Tau E	19.1	0.16	0.05	0.40	0.10	0.7
GW Ori	242	1.1	0.45	2.0	0.07[b]	0.6[b]
					>7:[c]	...

[a] Minimum radius for the outer extent of the CO emission.
[b] Broad component of the GW Ori line profile (see text).
[c] Narrow component of the GW Ori line profile (see text).

The CO fundamental 1–0 line profiles in GW Ori have both broad and narrow components, and the average line width increases toward the more energetic transitions (Table 5). The width of the broad component in the 1–0 $P(26)$ line is 39 km s^{-1} HWHM with a maximum velocity in the wing of $\gtrsim$80 km s^{-1}. The 2–1 lines are broader: the average HWHM of the 2–1 $R(10)$ and $R(11)$ lines is 63 km s^{-1}. The narrow component is either barely resolved or unresolved at our resolution (15 km s^{-1}). The system inclination was estimated to be 27° by Mathieu et al. (1991), although this value is highly uncertain.

Given this inclination, the broad component of the 1–0 emission would arise from an inner radius $\lesssim$0.07 AU and an outer radius $\geq$0.6 AU, for motion about the primary star. The 2–1 emission would have to extend to at least 0.2 AU. Because the narrow component is not clearly resolved, its location is not well determined. If it originates in the disk, it must clearly do so at large radii; e.g., a velocity of 8 km s^{-1} corresponds to a radius of 7 AU. Thus, the CO emission is unlikely to originate from a gap of the expected radii. For a gap extending from 0.45 to 2 AU, the line profile would have a maximum velocity of 32 km s^{-1} and an HWHM of 21 km s^{-1} or, for a gap extending from 0.17 to 3.3 AU (as implied by the SED modeling), a maximum velocity of 52 km s^{-1} and an HWHM of 17 km s^{-1}. These velocities are inconsistent with the observed profiles. Instead, the radii associated with the narrow and broad components bracket the $\sim$1.1 AU orbital separation of the binary and plausibly correspond to emission from a circumbinary disk and one or two circumstellar disks, respectively.

Mathieu et al. (1991) noticed a velocity variation of the binary center of mass, suggestive of a tertiary component, and subsequent observations (R. D. Mathieu & D. W. Latham 2003, unpublished) show this variation to have a period of several thousand days. If a tertiary star is present, the inner edge of the circumbinary disk would have a larger radius than predicted by Mathieu et al. (1991), arguably consistent with the narrow 1–0 component. A tertiary star would also make the mass accretion flow from the circumbinary disk much more complex than that considered by Artymowicz & Lubow (1994), which may explain the absence of CO fundamental emission from within the gap.

Hence, the short-period binaries present a different picture for the origin of the CO emission than does GW Ori. The CO line widths in DQ Tau and UZ Tau E imply strong emission from within the expected gap or inner hole in these systems (and perhaps emission from larger radii as well). In GW Ori, the profiles require an absence of emission from the gap and strong emission from the radii where optically thick disks are expected. Interestingly, the SEDs of both DQ Tau and UZ Tau are power laws in the infrared (Mathieu et al. 1997; Jensen, Koerner, & Mathieu 1996) and show no sign of a dip as expected from a lack of material in a gap; the presence of strong CO emission could be consistent with the idea that sufficient material is present in the gap to fill in the SED (Mathieu et al. 1997; Jensen & Mathieu 1997). In contrast, the SED for GW Ori is consistent with a large disk gap (Mathieu et al. 1991), and a lack of CO emission from the gap would support a conclusion that the region is relatively devoid of material.

5.3.2. *Single Stars*

For the single stars and spatially resolved binaries, a discussion of the disk radii for the CO emission must be restricted to the stars that have inclination estimates. Four of the CO emission stars (LkCa 15, GG Tau A, BP Tau, and CY Tau) have measurements of the stellar mass and inclination from the CO interferometric observations of Simon et al. (2000). Two other stars (GK Tau and IQ Tau) have accurate stellar rotation periods and measured stellar rotational velocities $v_* \sin i$ that can be combined with estimates of the stellar radius to give an inclination. For these two stars, the stellar effective temperature and luminosity were taken from Kenyon & Hartmann (1995). The stellar rotation periods P_* of the stars are listed in Table 8. The values of $v_* \sin i$ were taken from Hartmann & Stauffer (1989) and Johns-Krull & Valenti (2001). The masses for GK Tau and IQ Tau were estimated from the pre–main-sequence tracks of Siess, Dufour, & Forestini (2000), and a temperature error corresponding to one spectral subclass was used to assign an error to the mass. The mass M_* and inclination i for the six stars are listed in Table 8. The values that are estimated from the stellar parameters are more uncertain than the results from Simon et al. (2000). Table 8 gives the maximum velocity $V_{\rm max}$ as measured in the wing of the 1–0 $P(26)$ line, the corresponding inner CO emission radius $R_{\rm in}$, and the minimum value for the outer CO radius $R_{\rm out}$(min) based on the HWHM velocity.

It is interesting to compare $R_{\rm in}$ with the corotation radius R_c (Table 8, seventh column). Equilibrium magnetospheric

TABLE 8
Single-Star Parameters and CO Emission Radii

Star	P_*[a] (days)	M_* ($M_\odot$)	i	$V_{\rm max}$ (km s^{-1})	$R_{\rm in}$ (AU)	R_c[b] (AU)	$R_{\rm out}$(min)[c] (AU)
LkCa 15	5.85	0.97[d]	52[d]	80 ± 20	0.093	0.083	0.78
GG Tau A	10.3	0.8[e]	37[d]	105 ± 10	0.023	0.086	0.23
BP Tau	7.6	1.24[d]	30[d]	80 ± 5	0.043	0.081	0.44
CY Tau	7.5	0.55[d]	30[d]	60 ± 10	0.034	0.062	0.17
GK Tau	4.65	0.75[f]	52[g]	96 ± 5	0.045	0.050	0.62
IQ Tau	6.25	0.52[f]	49[g]	80 ± 10	0.041	0.054	0.21

[a] Periods from the compilation in Bouvier et al. 1995.
[b] Corotation radius.
[c] Minimum radius for the outer extent of the CO emission.
[d] Simon et al. 2000.
[e] Simon et al. 2000; assumed 0.8 $M_\odot$ for the mass of Aa.
[f] Mass derived from stellar evolutionary tracks (see text).
[g] Inclination obtained from P_*, $v \sin i$, T_*, and L_*.

accretion models for T Tauri stars truncate the inner disk a few stellar radii from the star, at approximately R_c, where the rotation period of the disk is equal to the stellar rotation period. We compare R_{in} and R_c in Figure 11. For LkCa 15, R_{in} has a large error due to the very low S/N in the line profile and the resulting large uncertainty in the velocity extent of the line. For the other stars, R_{in} is 0.02–0.05 AU (i.e., $\sim 2R_*$–$5R_*$) and $R_{in} \leq R_c$. The dotted line in Figure 11 shows the locus for Keplerian rotation at one-half the corotation radius; $R_{in} \simeq 0.5R_c$–$1.0R_c$ for most of the stars.

If the inner CO emission radius is equal to the disk truncation radius, then T Tauri star disks are typically truncated within corotation. This result would have implications for magnetospheric accretion theories. For example, the popular Shu et al. (1994) model places the truncation radius very close to the corotation radius. Kenyon, Yi, & Hartmann (1996) found a similar result in attempting to fit the observed infrared colors of T Tauri stars, i.e., that the truncation radius is $\simeq 0.4R_c$–$0.8R_c$. These values are similar to the values of R_{in}/R_c that we find. However, it is important to keep in mind that the emission profile wings are assumed to arise from gas in a Keplerian disk, but CO emission from other circumstellar components, or non-Keplerian motions, could confuse the interpretation. Since very little gas is required to produce the emission, a small amount of dynamically unimportant material within the truncation radius could explain the line wings. Hence, while the CO emission may be able to provide vital information on where disks are truncated, further work is needed before drawing definite conclusions.

For the six stars, we find $R_{out}(\min) = 0.2$–0.8 AU. Given that these are minimum outer radii and that emission over a large range in radius is required to produce centrally peaked profiles, the CO emission probably extends to 1–2 AU in most of the stars. It is perhaps surprising that the emission extends this far out, since gas temperatures of $\sim$500 K are required at these radii in order to produce the 1–0 emission. In contrast, the typical disk effective temperature at 1 AU for the T Tauri stars in our sample is $\sim$130 K; at 0.04 AU, the typical disk effective temperature is $\sim$900 K (Beckwith et al. 1990). This result implies substantial temperature inversions at $\sim$1 AU, and the frequency of CO fundamental emission implies that strong temperature inversions are common in the atmospheres of inner T Tauri disks.

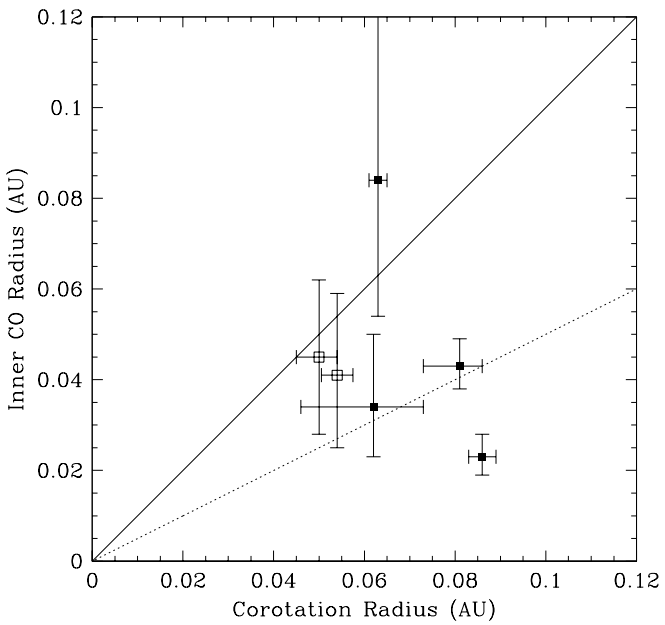

FIG. 11.—Comparison of the inner CO emission radius and the corotation radius for the single stars in our sample for which inclination estimates are available either from CO interferometric measurements (*filled symbols*) or stellar rotational velocities and periods (*open symbols*). The solid and dotted lines indicate an inner emission radius equal to 1.0 and 0.5 times the corotation radius, respectively.

Additional observational evidence for warm disk atmospheres may come from the detection of UV fluorescence Lyman-band H_2 emission from T Tauri stars, which has been postulated to arise in a disk (e.g., Herczeg et al. 2002; J. Valenti 2001, private communication). The fluorescence emission occurs from excited rovibrational levels of warm ($\sim$2000–3500 K) H_2. Since the widths of the lines are fairly narrow, if the emission arises in a disk, the emission occurs from large disk radii. For example, the H_2 emission from DF Tau has an FWHM of $\sim$25 km s^{-1} (Herczeg et al. 2002), much narrower than the $\sim$70 km s^{-1} width found for the CO fundamental lines from this source. For the mass and inclination of the DF Tau system, the H_2 line width suggests that the emission arises at disk radii greater than 3 AU. Taken at face value, the H_2 results suggest that warm ($\sim$2000 K) gas is present at disk surfaces at AU distances. The disk interpretation of these H_2 results and the CO fundamental results presented here, if true, imply that the processes that heat disk atmospheres are more efficient than previously believed.

5.3.3. *Vertical Temperature Structure of Disks*

The vertical temperature structure of T Tauri disk atmospheres heated by radiation from the central star has been studied theoretically by several groups, for both actively accreting (Calvet et al. 1991; Malbet & Bertout 1991; D'Alessio et al. 1998; Malbet, Lachaume, & Monin 2001) and passive circumstellar disks (Chiang & Goldreich 1997; Chiang et al. 2001; Dullemond, van Zadelhoff, & Natta 2002). A vertical temperature inversion at all disk radii is a common result of these studies.

An important issue in understanding the origin of the CO fundamental emission is whether gas in the upper disk atmosphere is warm enough over the vertical region in which CO resides. At a fiducial radius of 1 AU, the theoretical studies of disk atmospheres predict temperature inversion regions of 200–400 K, compared to a disk photospheric temperature of $\sim$130 K at the same radius. These temperatures appear low when compared to those needed to produce CO emission at AU distances. An additional concern is the column density of warm gas in the inversion region, which is also low compared to that required to produce the observed CO line fluxes.

However, the disk atmosphere calculations to date refer primarily to the temperature structure in the dust component of the disk. Indeed, Chiang & Goldreich (1997) have emphasized that the gas and dust components are thermally uncoupled in the upper disk atmosphere. There, the dust temperature is determined by the absorption and reradiation of stellar photons, whereas the gas temperature is regulated by collisions with dust grains and other heating and cooling processes. Thus, the vertical temperature structure of the gas in the upper disk atmosphere requires its own calculation.

Glassgold & Najita (2001) have considered the vertical temperature structure of the gaseous component at AU distances and have suggested that heating by stellar X-ray irradiation can drive a vertical temperature inversion in the gas. Because of the efficiency of heating by X-rays at low densities, the gas is actually expected to reach higher temperatures than the dust in the upper disk atmosphere. In contrast to the dust temperature inversion, which relies on the presence of small grains in the disk atmosphere, the gas temperature inversion is relatively insensitive to the rates of grain growth and settling. More detailed calculations of the vertical structure of the gaseous component are needed to determine whether disk atmospheres heated by X-rays (or other physical processes such as Alfvén-wave heating) can produce the temperatures and column densities needed to explain the strength and line profiles of the CO fundamental lines.

Also required in order to compare the observations with disk atmosphere models is an analysis of the vertical chemical structure of disk atmospheres. This is needed both to determine where in the disk atmosphere CO resides and whether collisions there are frequent enough to explain the observed emission. For example, X-ray irradiation of the disk surface will destroy molecules such as CO. The subsequent formation of CO in warm disk atmospheres (>a few 100 K) may be somewhat difficult because the familiar grain-catalyzed formation process for H_2 (a necessary chemical precursor for CO) is inefficient at warm temperatures (e.g., Cazaux & Tielens 2002). Instead, CO may be produced through a much slower gas-phase synthesis process (e.g., Glassgold & Najita 2001). If, as suggested by these authors, the transition from atomic carbon to CO is made higher up in the atmosphere than the transition from atomic to molecular hydrogen, CO may be mixed with atomic hydrogen over a significant column density of the disk. This situation is advantageous for the excitation of CO, since the collisional cross section for exciting CO with H is much larger than the cross section for exciting CO with H_2 (e.g., Najita et al. 1996).

5.4. CO *Emission from a Transitional T Tauri Star*

One of our more interesting results is the detection of CO fundamental emission from V836 Tau, a T Tauri star with properties intermediate between those of weak and classical T Tauri stars. The consequent status of V836 Tau as a "transitional T Tauri star" (e.g., Skrutskie et al. 1990) reflects the assumption that classical T Tauri stars evolve into weak T Tauri stars with the dissipation of the disk playing a central role in that evolutionary process. For example, the small but variable Hα equivalent width (1–15 Å; Mundt et al. 1983; Wolk & Walter 1996; Beristain, Edwards, & Kwan 2001) places V836 Tau among the weak T Tauri stars. Similarly, the star experiences very little veiling and has one of the smallest measured accretion rates among T Tauri stars (Hartigan et al. 1995). However, the detection of an inverse P Cygni profile from the source (Wolk & Walter 1996) reveals the continued (possibly intermittent) accretion of material onto the star. In the infrared, V836 shows little or no excess at 2.2 μm, an intermediate $K-L$ color, and an excess indicative of an optically thick disk at wavelengths beyond 10 μm (Strom et al. 1989; Skrutskie et al. 1990; Hartigan et al. 1995; Simon & Prato 1995; Wolk & Walter 1996). V836 Tau has also been detected in 1.3 mm continuum and CO $J = 2$–1 emission, the only one of 12 stars detected in a survey of millimeter emission from weak T Tauri stars (Duvert et al. 2000). Thus, observations from infrared to millimeter wavelengths indicate that V836 Tau has an optically thick outer disk, but the inner disk may have become optically thin, with a corresponding decrease in accretion activity. V836 Tau may, therefore, be one of the rare examples of a T Tauri system with a dissipating disk.

The weak CO fundamental emission from V836 Tau may also reflect the dissipation process in progress; i.e., the CO emission may arise from an optically thin inner disk. However, it is difficult to conclude this with certainty from the CO data alone because, from an empirical standpoint, we also found weak emission from other classical T Tauri stars (e.g., LkCa 15) and did not detect the classical T Tauri star GM Aur. Thus, CO fundamental emission strength may not correlate directly with gas mass at early times when disks are optically thick in the continuum. Indeed, a correlation is not expected in the context of disk atmospheres since only the portion of the atmosphere that participates in the temperature inversion would produce emission.

However, CO fundamental emission may become a good tracer of disk gas mass at late times, when the inner disk has become optically thin in the continuum. Indeed, infrared SEDs of T Tauri stars indicate that inner disks become optically thin on timescales less than a few Myr. This may be the result of grain growth (or the agglomeration of dust into larger bodies) or is perhaps due to the dispersal of the inner disk (e.g., by the accretion of the gas and dust onto the star). One way to distinguish between these possibilities is to measure the gas content of inner disks. Because fundamental emission from CO and its isotopes is sensitive to a wide range of gas masses (e.g., the CO emission from DQ Tau corresponds to only 10^{-5} $M_\oplus$ of gas), CO fundamental emission may prove useful in measuring the residual gas content in dissipating disks. This may be an effective way to explore the gas dissipation timescale in inner disks and to thereby place constraints on the timescale for giant planet formation.

6. SUMMARY AND CONCLUSIONS

We find that CO fundamental emission is frequently detected in T Tauri stars, with the likely origin of the emission in the circumstellar disk. The strength of the emission is correlated with indicators for disk accretion, suggesting an association with circumstellar disks. More specifically, the generally symmetric profile shapes and the profile widths strongly favor a disk origin. An initial assessment of the line profiles indicates that the emission arises from a large range of disk radii, from the immediate vicinity of (and perhaps within) the corotation radius ($\sim$0.05 AU) to disk radii $\gtrsim$1 AU. Since fundamental emission is detected frequently from both binary and apparently single stars, it appears that both low column density regions (gaps) and temperature inversion regions in disk atmospheres can produce significant emission. Based on the relative integrated line strengths of the CO lines, we find a high excitation temperature for the emitting gas of $\sim$1000 K and possibly significant optical depth in some sources. The high gas temperature is surprising given the distances probed by the emission. Thus, the surface gaseous component of inner disks may be heated to higher temperatures than the surface dust component.

The detection of gas in the circumstellar environment of close binaries supports earlier evidence for ongoing accretion in these systems. Classical dynamical theory suggests

that the clearing of gaps by stellar companions would also terminate mass accretion flows from circumbinary disks. However, numerous observational diagnostics suggest that mass accretion continues onto the surfaces of stars in binaries and that the lifetimes of circumstellar disks in binaries are comparable to those around single stars (e.g., Mathieu 2001). Our observations of CO fundamental emission from both the gap regions and from circumstellar disks of the binaries DQ Tau, UZ Tau E, and GW Ori further confirm the ongoing inward flow of disk material from circumbinary disks.

More importantly, it appears that with the CO fundamental lines, we can effectively extend spectroscopic studies of disks beyond the region probed by the CO overtone lines and hot water lines in the *K* band. Given the wide range of excitation temperatures and column densities that can be probed by the fundamental lines of CO and its isotopes, fundamental emission may prove to be a useful probe of the dynamics and physical properties of disks within a few AU of the central star. This is an interesting range of radii since it overlaps the terrestrial planet formation region as well as the range of radii currently probed by precision radial velocity searches for extrasolar planets.

One of our more interesting results is the detection of CO fundamental emission from a transitional T Tauri star, a result that suggests the possibility of using CO fundamental emission to explore the gas dissipation timescale in inner disks and thereby place constraints on the timescale for giant planet formation. Since multiple physical processes may reduce the continuum optical depth of inner disks, using CO to measure the gas content of inner disks may also aid in distinguishing between ongoing grain agglomeration (and potential planet building) and disk dispersal in the terrestrial planet formation region of disks.

One of the interesting results emerging from precision radial velocity searches is the distribution of planetary orbital radii, which is rising beyond 1 AU, suggesting large numbers of undiscovered planets at orbital separations of $\gtrsim$a few AU (G. Marcy 2002, private communication).[2] This, and the theoretical expectation that giant planets form at $\sim$5 AU, is significant motivation to extend spectroscopic studies of young disks beyond the distances probed by CO fundamental emission. Of the possible diagnostics, the most appealing, perhaps, are the pure rotational lines of H_2. Thus far, these lines have been detected in emission by the *Infrared Space Observatory* (*ISO*) in T Tauri stars and debris disk systems (Thi et al. 1999, 2001). If the emission arises in a disk,[3] both the smaller characteristic temperature of the H_2 emission ($\sim$100 K) compared to the CO emission ($\sim$1000 K) and the large H_2 line fluxes reported indicate that much of the emission comes from a region much larger than a few AU in size. Extending these studies to much smaller H_2 line fluxes and to high spectral resolution may enable the spectroscopic study of disks in the region of $\sim$5 AU.

The authors wish to recognize and acknowledge the very significant cultural role and reverence that the summit of Mauna Kea has always had within the indigenous Hawaiian community. We are most fortunate to have the opportunity to conduct observations from this mountain. It is a great pleasure to thank our Keck instrument specialists David Sprayberry and Bob Goodrich and our OAs Terry and Gabrelle for their help in calibrating and implementing the stationary guiding mode used in acquiring the data. The NIRSPEC data in this paper were obtained at the W. M. Keck Observatory, which is operated as a scientific partnership among the California Institute of Technology, the University of California, and the National Aeronautics and Space Administration. The Observatory was made possible by the generous financial support of the W. M. Keck Foundation. We would also like to thank Jeff Valenti for sharing his Marquardt fitting routine. J. S. C. acknowledges support from the NASA Origins of Solar Systems program and the Office of Naval Research.

[2] See also http://exoplanets.org.

[3] Currently there is uncertainty as to whether the *ISO* H_2 emission truly arises in a disk or from a much more extended region of $\gtrsim 5''$, since ground-based searches for H_2 emission from some of the same T Tauri systems do not detect emission close to the star (Richter et al. 2002).

REFERENCES

Artymowicz, P., & Lubow, S. H. 1994, ApJ, 421, 651
Basri, G., & Batalha, C. 1990, ApJ, 363, 654
Basri, G., Johns-Krull, C., & Mathieu, R. 1997, AJ, 114, 781
Beckwith, S., Sargent, A., Chini, R., & Gusten, R. 1990, AJ, 99, 924
Beristain, G., Edwards, S., & Kwan, J. 2001, ApJ, 551, 1037
Biscaya, A., Rieke, G., Narayanan, G., Luhman, K., & Young, E. 1997, ApJ, 491, 359
Bouvier, J., Covino, E., Kovo, O., Martin, E. L., Matthews, J. M., Terranegra, L., & Beck, S. C. 1995, A&A, 299, 89
Brittain, S. D., & Rettig, T. W. 2002, Nature, 418, 57
Calvet, N., Patiño, A., Magris, G., & D'Alessio, P. 1991, ApJ, 380, 617
Carr, J., & Najita, J. 1998, in ASP Conf. Ser. 133, Science with the *NGST* (*Next Generation Space Telescope*), ed. E. P. Smith & A. Koratkar (San Francisco: ASP), 163
Carr, J. S. 1989, ApJ, 345, 522
Carr, J. S., Mathieu, R. D., & Najita, J. R. 2001, ApJ, 551, 454
Carr, J. S., Tokunaga, A. T., Najita, J., Shu, F. H., & Glassgold, A. E. 1993, ApJ, 411, L37
Cazaux, S., & Tielens, A. G. G. M. 2002, ApJ, 575, L29
Chandler, C. J., Carlstrom, J. E., & Scoville, N. Z. 1995, ApJ, 446, 793
Chiang, E. I., & Goldreich, P. 1997, ApJ, 490, 368
Chiang, E. I., Joung, M., Creech-Eakman, M., Qi, C., Kessler, J., Blake, G., & van Dishoeck, E. 2001, ApJ, 547, 1077
D'Alessio, P., Cantó, J., Calvet, N., & Lizano, S. 1998, ApJ, 500, 411
Dullemond, C., van Zadelhoff, G., & Natta, A. 2002, A&A, 389, 464
Dutrey, A., Guilloteau, S., Duvert, G., Prato, L., Simon, M., Schuster, K., & Ménard, F. 1996, A&A, 309, 493
Duvert, G., Guilloteau, S., Ménard, F., Simon, M., & Dutrey, A. 2000, A&A, 355, 165
Edwards, S., Hartigan, P., Ghandour, L., & Andrulis, C. 1994, AJ, 108, 1056
Glassgold, A. E., Mamon, G. A., & Huggins, P. J. 1991, ApJ, 373, 254
Glassgold, A. E., & Najita, J. R. 2001, in ASP Conf. Ser. 244, Young Stars near Earth: Progress and Prospects, ed. R. Jayawardhana & T. Greene (San Francisco: ASP), 251
Greene, T. P., & Lada, C. J. 1996, AJ, 112, 2184
Greene, T. P., Tokunaga, A. T., Toomey, D. W., & Carr, J. S. 1993, Proc. SPIE, 1946, 313
Gullbring, E., Calvet, N., Muzerolle, J., & Hartmann, L. 2000, ApJ, 544, 927
Gullbring, E., Hartmann, L., Briceno, C., & Calvet, N. 1998, ApJ, 492, 323
Hamann, F., Simon, M., & Ridgway, S. 1988, ApJ, 326, 859
Hartigan, P., Edwards, S., & Ghandour, L. 1995, ApJ, 452, 736
Hartigan, P., Hartmann, L., Kenyon, S., Strom, S., & Skrutskie, M. 1990, ApJ, 354, L25
Hartmann, L., Calvet, N., Gullbring, E., & D'Alessio, P. 1998, ApJ, 495, 385
Hartmann, L., Hewett, R., & Calvet, N. 1994, ApJ, 426, 669
Hartmann, L., & Stauffer, J. 1989, AJ, 97, 873
Herczeg, G. J., Linsky, J. L., Valenti, J. A., Johns-Krull, C. M., & Wood, B. E. 2002, ApJ, 572, 310
Jensen, E. L. N., Koerner, D. W., & Mathieu, R. D. 1996, AJ, 111, 2431
Jensen, E. L. N., & Mathieu, R. D. 1997, AJ, 114, 301
Johns-Krull, C., & Valenti, J. 2001, ApJ, 561, 1060

Kenyon, S. J., & Hartmann, L. 1995, ApJS, 101, 117
Kenyon, S. J., Yi, I., & Hartmann, L. 1996, ApJ, 462, 439
Krotkov, R., Wang, D., & Scoville, N. Z. 1980, ApJ, 240, 940
Luhman, K. L., & Rieke, G. H. 1998, ApJ, 497, 354
Malbet, F., & Bertout, C. 1991, ApJ, 383, 814
Malbet, F., Lachaume, R., & Monin, J.-L. 2001, A&A, 379, 515
Martin, S. C. 1996, ApJ, 470, 537
———. 1997, ApJ, 478, L33
Mathieu, R. D. 2001, in IAU Symp. 200, Formation of Binary Stars, ed. H. Zinnecker & R. D. Mathieu (San Francisco: ASP), 419
Mathieu, R. D., Adams, F. C., & Latham, D. W. 1991, AJ, 101, 2184
Mathieu, R. D., Martín, E. L., & Magazzu, A. 1996, BAAS, 28, 920
Mathieu, R. D., Stassun, K., Basri, G., Jensen, E. L. N., Johns-Krull, C. M., Valenti, J. A., & Hartmann, L. W. 1997, AJ, 113, 1841
McLean, I. S., Becklin, E. E., Bendiksen, O., Brims, G., & Canfield, J. 1998, Proc. SPIE, 3354, 566
McLean, I. S., Graham, J. R., Becklin, E. E., Figer, D. F., Larkin, J. E., Levenson, N. A., & Teplitz, H. I. 2000, Proc. SPIE, 4008, 1048
Mundt, R., Walter, F. M., Feigelson, E. D., Finkenzeller, U., Herbig, G. H., & Odell, A. P. 1983, ApJ, 269, 229
Muzerolle, J., Calvet, N., & Hartmann, L. 1998, ApJ, 492, 743
———. 2001, ApJ, 550, 944
Najita, J., Carr, J. S., Glassgold, A. E., Shu, F. H., & Tokunaga, A. T. 1996, ApJ, 462, 919
Najita, J. R., Edwards, S., Basri, G., & Carr, J. 2000, in Protostars and Planets IV, ed. V. Mannings, A. P. Boss, & S. S. Russell (Tucson: Univ. Arizona Press), 457
Ostriker, E., & Shu, F. 1995, ApJ, 447, 813
Prato, L., Simon, M., Mazeh, T., Zucker, S., & McLean, I. S. 2002, ApJ, 579, L99
Richter, M. J., Jaffe, D. T., Blake, G. A., & Lacy, J. H. 2002, ApJ, 572, L161
Shu, F., Najita, J., Ostriker, E., Wilkin, F., Ruden, S., & Lizano, S. 1994, ApJ, 429, 781
Siess, L., Dufour, E., & Forestini, M. 2000, A&A, 358, 593
Simon, M., Dutrey, A., & Guilloteau, S. 2000, ApJ, 545, 1034
Simon, M., & Prato, L. 1995, ApJ, 450, 824
Skrutskie, M. F., et al. 1990, AJ, 99, 1187
Strom, K. M., Strom, S. E., Edwards, S., Cabrit, S., & Skrutskie, M. F. 1989, AJ, 97, 1451
Thi, W. F., van Dishoeck, E. F., Blake, G. A., van Zadelhoff, G. J., & Hogerheijde, M. R. 1999, ApJ, 521, L63
Thi, W. F., et al. 2001, ApJ, 561, 1074
Tokunaga, A. T., Toomey, D. W., Carr, J. S., Hall, D. N. B., & Epps, H. W. 1990, Proc. SPIE, 1235, 131
Valenti, J., Basri, G., & Johns, C. 1993, AJ, 106, 2024
White, R. J., Ghez, A. M., Reid, I. N., & Schultz, G. 1999, ApJ, 520, 811
Wolk, S. J., & Walter, F. M. 1996, AJ, 111, 2066